The Study of Molecular Spectroscopy by ab Initio Methods

CHARLES W. BAUSCHLICHER, JR.* and STEPHEN R. LANGHOFF*

NASA Ames Research Center, Moffett Field, California 94035

Received October 30, 1990 (Revised Manuscript Received February 11, 1991)

Contents

Charles W. Bauschlicher, Jr. is a research scientist at NASA Ames Research Center. He received his B.S. degree in 1972 from SUNY at Stony Brook and his Ph.D in 1976 from the University of California at Berkeley, where he worked under the direction of H. F. Schaefer. After postdoctoral research at Battelle with I. Shavitt, he jointed NASA in 1977, becoming a permanent staff member in 1982. Dr. Bauschlicher's research interests center on understanding the structure and spectroscopy of small molecules, especially those containing metal atoms.

Stephen R. Langhoff is a research scientist at NASA Ames Research Center. He received his B.S. degree in 1968 from Colorado College and his Ph.D. degree in 1973 from the University of Washington, where he worked under the direction of E. R. Davidson. After postdoctoral research with W. C. Kern at Battelle Memorial Laboratory he joined NASA in 1976. His research effort is centered on developing and benchmarking theoretical methods for determining accurate spectroscopic constants and properties of small molecules. Although interested in a wide range of problems in molecular spectroscopy, his research interests are now centered on transition-metal systems.

I. Introduction

Spectroscopy is capable of yielding a wealth of information, not only about the energy levels of a molecule over a wide wavelength region, but also about molecular structure and the nature of the bonding. For example, the moments of inertia can be deduced from a rotational analysis, thereby yielding accurate bond lengths. Both electronic and vibrational spectroscopy give considerable insight into the bonding and how it changes with molecular environment. Since every band system of a molecule is unique, it provides an excellent fingerprint for molecular systems, thereby making spectroscopy a particularly important means of studying molecules in interstellar space.

Unfortunately an experimental spectrum can be very difficult to assign, even when the identity of the molecular species is certain, often because of the complexity resulting from a very high density of states. While high-resolution spectroscopy is capable of yielding spectroscopic constants for diatomic molecules of far greater accuracy than even the best ab initio calculations, theory is sufficiently accurate to complement experiment and to yield considerable insight into the nature of the bonding. Improvements in the accuracy of theoretical calculations have come not only from advances in theoretical methods and computer hardware, but from a greater understanding of the accuracy of ab initio methods. Given the rapid improvement in ab initio methods over the last few years, it seems timely to review the current state-of-the-art computational approaches to solving spectroscopic problems.

The area of spectroscopy is far too large to cover every aspect or to give a comprehensive survey of the literature. In this review we focus primarily on radiative

transitions, but nonradiative processes can also be important in determining the lifetimes. See, for example, the study of the lifetime of the $b^4\Sigma_g^-$ state of O_2^+ by Marian et al.,[1] where the computed predissociation rate is in good agreement with that extracted from experiment. Radiationless transitions can also occur as a result of nonadiabatic processes such as curve crossings. To determine whether the adiabatic or diabatic representation is preferable requires knowledge of the nonadiabatic coupling matrix elements (NACMEs). Recently Lengsfield, Saxe, and Yarkony[2,3] have developed an efficient method for evaluating the NACMEs based on state-averaged multiconfiguration self-consistent-field (MCSCF) functions and analytic derivative methods. Therefore it is currently possible to handle the most important nonradiative processes when these are the dominant decay channels. In this review we give several examples of the application of ab initio calculations to rotational, vibrational, and electronic spectroscopy. In section II we discuss the computational methods used. In sections III, IV, and V we give examples of rotational, vibrational, and electronic spectroscopy, respectively. Section VI contains our conclusions.

II. Computational Methods

Our main goal is to illustrate the level of accuracy currently achievable with ab initio methods. We discuss the level of theory required to solve different types of spectroscopic problems. However, it is not our goal to summarize all computational methods currently in use, as this has been the subject of other reviews.[4] In this section we give an overview of the methods that are used in determining the electronic energy and wave function. The methods for the calculation of vibrational levels, lifetimes, and construction of spectra are deferred to subsequent sections.

In the molecular orbital picture, the Schrödinger equation is solved approximately in the Born–Oppenheimer approximation by using a double basis set expansion. The accuracy of calculations is determined by the approximations used in selecting the one-particle (the orbital basis set) and n-particle (correlation treatment) basis sets. Full configuration–interaction (FCI) benchmark calculations have shown that the computational requirements for obtaining accurate results depend greatly on the specific system and property of interest. This is described in detail in ref 5.

An important recent methodological advancement is the atomic natural orbital (ANO) approach[6] of contracting one-particle basis sets. It is particularly useful in benchmark calculations, because it offers a systematic means of expanding the one-particle basis set, and thereby demonstrating convergence of a property. However, very large segmented basis sets are also capable of yielding accurate results. Some discussion of one-particle basis sets is included in specific examples below.

In both rotational and vibrational spectroscopy the ground-state energy and dipole moment for geometries near equilibrium are the quantities that are needed to characterize transitions between the lowest levels. Near equilibrium many molecules are well described by a single configuration, and qualitative information can be obtained at the SCF level. The accuracy can be dramatically improved with the inclusion of correlation even at the lowest levels of theory. A method that has proved to be quite useful is Møller–Plesset second-order (MP2) perturbation theory.[7] An advantage of this method is that it is possible to economically implement the analytic evaluation of the second derivatives,[8] which are needed to determine the force field for molecular systems. The singles and doubles configuration–interaction (SDCI) approach has also been applied to this class of problems. However, better accuracy is generally achieved by using a method that is at least approximately size extensive. These include the coupled-cluster (CC)[9] and the coupled-pair functional (CPF)[10] (and its modified form MCPF[11]) approaches. The CC approach also has the advantage that the effect of triple excitations[12,13] can be estimated from perturbation theory. An advantage of the CPF or MCPF methods is that the dipole moment can be determined as an expectation value at virtually no additional computational expense.

Degenercies that can dramatically reduce the accuracy of single-reference-based approaches can be easily accounted for by using the complete active space self-consistent field (CASSCF) procedure. Such degeneracies may arise, for example, when the bond lengths or angles are displaced greatly. More extensive correlation can subsequently be added by using a multireference configuration–interaction (MRCI) approach. As long as the most important correlation effects are included in the CASSCF active space, the CASSCF/MRCI approach is capable of describing the entire surface equally well. Thus CASSCF/MRCI based approaches are often optimal when highly vibrationally excited levels of a molecule are investigated.

To characterize spectroscopic transitions between Born–Oppenheimer surfaces requires the calculation of the electronic transition moment function (TMF) for all relevant geometries. This is complicated by the fact that two electronic states are involved. Thus one must either deal with two different sets of molecular orbitals or use a common set for both states. An excellent method of determining a compromise set of orbitals is the state-averaged (SA) CASSCF approach, which allows the optimization of the orbitals for the average energy of two (or more) states. In this way all states are treated approximately equally.

Recent advances[14,15] in the CASSCF procedure have dramatically expanded the size of the systems that can be treated and how much correlation can be accounted for in the CASSCF procedure, or its restricted (RASSCF) version.[16] The accuracy of the CASSCF approach can be further improved by using different orbitals for each state of interest. For many systems this gives accurate spectroscopic properties without the inclusion of more extensive correlation through a subsequent MRCI calculation. It should be noted that despite the use of nonorthogonal orbitals, the transition moments can be computed very efficiently for CASSCF wave functions.[17] Thus this approach offers an alternative to the SA-CASSCF/MRCI approach.

To obtain very accurate TMFs or potential energy curves, it is necessary to include a substantial fraction of the nondynamical (external) correlation. The CASSCF/MRCI method has been shown to reproduce the FCI results very closely for a wide range of spectroscopic problems.[5] The accuracy of this level of

theory can be further improved in many cases by using the averaged CPF (ACPF) method,[18] which is a multireference analogue of the CPF approach, to account for higher excitations. Experience has shown that only the configurations with the largest coefficients in the CASSCF wave function need to be included in the MRCI reference space. A threshold of 0.05 in the reference selection process is usually sufficient to reproduce the full CAS-ref (i.e. no reference selection) results.

CI expansions of several million can easily be handled by using the direct CI approach on current computer hardware. This means that very large basis sets and relatively small (0.01–0.05) reference thresholds can be routinely used for small molecules. However, the CI expansions still become intractably long for many problems, especially when several roots of the Hamiltonian matrix are desired. For example, in many transition-metal compounds, the density of states is so large that to characterize transitions in the visible region often involves obtaining several roots of a given symmetry. Reducing the size of the one-particle basis set or increasing the selection threshold to reduce the length of the CI expansion can significantly reduce the accuracy of the calculations. An alternative is to select individual configurations based on perturbation theory. While this conventional CI approach with selection[19] is less accurate (and precise) than the direct CI, it is still capable of yielding high-quality results.

III. Rotational or Microwave Spectroscopy

Microwave radiation is absorbed or emitted when a molecule changes rotational level. Since the intensity is proportional to the dipole moment, rotational spectroscopy is applicable to all molecules that possess a permanent dipole moment. For a $^1\Sigma$ state of a diatomic molecule the rotational frequencies for $v = 0$ are given as

$$\nu(J,J+1) = 2B_0(J+1) - 4D_0(J+1)^3 \qquad (1)$$

For the low rotational levels, D_0 can be neglected and hence r_0 can be computed from the atomic masses and measured frequencies. However, when the identity of the molecule is unknown, its identification from the observed line position can be exceedingly difficult. This is frequently the case in the identification of new interstellar species. Theory can often provide sufficiently accurate r_0 values to define frequency regions for spectroscopic searches in both the laboratory and space. Probably the first successful application of theory to the identification of interstellar species is the study of HNC by Pearson et al.[20] Since then, the list of molecules where interstellar discovery or laboratory identification was corroborated or aided by theoretical studies has become quite extensive. For theory to be useful in the identification of unknown lines, molecular geometries must be computed very accurately. For small molecules, CASSCF/MRCI calculations in very large basis sets are probably sufficiently accurate to make a definitive assignment based on the calculations alone. However, this approach is not generally applicable for larger molecules.

One approach[21,22] to circumventing the difficulty of performing highly accurate calculations on larger systems is the extrapolation of the results at lower levels of theory. It is common to devise several such extrapolations to provide a criterion for their accuracy. For example, the computed B_e value can be scaled on the basis of a similar compound where experiment is known, i.e. $B_0(\text{expt})/B_e(\text{theory})$. This corrects for both limitations in the theory and vibrational effects (the difference between B_e and B_0). A second approach is to scale individual bond lengths on the basis of compounds with similar bonding. Furthermore, if these approaches are applied by using several levels of theory (for example MP2, MP4, and CISD), then there are consistency checks on the theoretical predictions.

An example of the application of extrapolation procedures is the work on C_3O, which has aided its identification in a laboratory spectrum.[23] In addition to yielding a rotational constant that is within 0.2% of experiment, the calculations showed that the molecule was quite stable. The molecule was subsequently identified in an interstellar molecular cloud. The next member of the series, C_5O, has also been the subject of theoretical study.[24] By using an approach similar to that used for C_3O, the extrapolated rotational constant is expected to be accurate to at least ±2%.

Some of the largest molecules that have been studied[24] to date have been the HC_nN series for odd n as large as 15. Those species with $n \leq 9$ have been observed in space. Longer-chain HC_nN species have not yet been observed, and theory can potentially aid in identification. However, for molecules of this size it is very difficult to include even the lowest levels of correlation, except possibly by using direct SCF and MP2 methods.[25] Therefore, the systems were studied by using the SCF approach, but considerably improved rotational constants were determined by extrapolation methods using the highly accurate experimental constants for $n = 3$–9. Given the large number of known molecules, the extrapolated value for $n = 11$ has been estimated to be accurate to 0.1%, which is sufficiently reliable that laboratory confirmation will not be necessary if the line can be observed in interstellar space.

In summary, while rotational spectroscopy has not been an extremely active area of theoretical study recently, it is one where there has been considerable interplay between theory and experiment. By using extrapolation schemes in conjunction with ab initio calculations, theory can determine approximate line positions to begin ground-based searches or laboratory experiments.

IV. Vibrational Spectroscopy

Vibrational spectroscopy is currently a very active area of theoretical study. As in the case of rotational spectroscopy, theory can be used to aid experiment in the identification of unknown molecules. Theory is also useful in assigning the modes or lines of known molecules, especially when there is a high degree of vibrational excitation. Theory has also contributed significantly to the prediction of intensities of vibrational transitions, as well as to determining the lifetimes of the individual vibrational levels that are important in modeling some processes.

The theoretical methods used to study the vibrational problem vary considerably with the size of the molecule. We begin our study with diatomic molecules for which the vibrational frequencies and transition strengths (lifetimes) require only the ground-state potential curve

and dipole-moment function (DMF). To compare with experimental observables such as oscillator strengths, Einstein coefficients, and band strengths, the DMF, $D(r)$, is integrated numerically over the nuclear coordinate r:

$$D_{v'v''} = \int_0^\infty \psi_{v'}(r)D(r)\psi_{v''}(r)\mathrm{d}r \qquad (2)$$

where $\psi_{v'}$ and $\psi_{v''}$ are the upper- and lower-state vibrational wave functions. The vibrational eigenfunctions can be determined by using either the theoretical or an experimentally derived potential. Although very accurate experimentally derived potentials exist for many species, experimentally derived DMFs tend to be far less accurate.

The strength of a transition between two vibrational states ($J' = J'' = 0$) is generally given in terms of the Einstein A coefficient (s^{-1}), which can be written as

$$A_{v'v''} = 2.026 \times 10^{-6}\, \bar{\nu}_{v'v''}{}^3 |D_{v'v''}|^2 \qquad (3)$$

where $D_{v'v''}$ is in atomic units and $\bar{\nu}_{v'v''}$ is the transition energy in cm^{-1} between levels v' and v''. The lifetime of a level is easily computed as the inverse of the sum of the Einstein coefficients to all lower levels.

A. OH: A Calibration Study of the One- and *n*-Particle Treatments

The rotational–vibrational bands of the $X^2\Pi$ state of OH, the Meinel system,[26] have been observed in many astrophysical sources,[27] and may be responsible for the surface-originating glow observed on the Atmosphere Explorer Satellites.[28] It is therefore disconcerting that there is still an uncertainty in the line strengths. Given the relatively small size of this system, FCI calculations correlating the seven valence electrons are possible in realistic one-particle basis sets. Thus it has been possible to assess the ability of a large number of truncated correlation methods to determine dipole moments and line strengths. In this section we discuss the details of our basis set study and FCI calibration[29] of the DMF of the $X^2\Pi$ state of OH.

We first studied the n-particle problem by comparing with FCI calculations using two relatively small basis sets.[29] In Table I we summarize the spectroscopic constants (r_e, ω_e, D_e) and the position of the maximum in the dipole moment function (r^{μ}_{max}) for many approximate correlation treatments. The use of two different basis sets minimizes the possibility of fortuitously good agreement.

The molecular orbitals were determined by using the CASSCF procedure. While we impose $C_{\infty v}$ symmetry and equivalence restrictions[30] in all CASSCF wave functions, the calculations are performed in C_{2v} symmetry. The CASSCF active space denoted in parentheses is labeled according to the number of active orbitals in the a_1, b_1, b_2, and a_2 symmetries. The MRCI calculations include all single and double excitations from all configurations in the CASSCF unless otherwise noted. We focus on the value of r^{μ}_{max}, as this quantity is most sensitive to the level of theory. The single reference-based SDCI technique gives a qualitatively incorrect DMF with an r^{μ}_{max} that is considerably too large. The CPF approaches improve the results, but

TABLE I. Comparison of OH $X^2\Pi$ Spectroscopic Constants with Level of Correlation Treatment[a]

	r_e, a_0	ω_e, cm^{-1}	D_e, eV	r^{μ}_{max}, a_0
[4s3p1d/2s1p] Basis				
FCI	1.855	3713.9	4.266	2.057
SDCI-FCI	−0.008	+59.0	−0.110	0.153
MCPF-FCI	−0.001	+1.8	−0.030	−0.039
CPF-FCI	−0.001	+5.2	−0.034	−0.021
(211)-CAS-FCI	−0.002	−71.9	−0.673	−0.166
(211)-CAS MRCI-FCI	−0.001	−1.8	−0.031	−0.026
(222)-CAS-FCI	+0.002	−44.4	−0.149	0.054
(222)-CAS MRCI(0.05)-FCI[b]	0.000	−0.9	+0.002	0.003
(222)-CAS MRCI-FCI	0.000	−2.2	−0.009	0.004
[4s3p2d/2s1p] Basis				
FCI	1.848	3708.7	4.395	2.271
SDCI-FCI	−0.009	−68.2	−0.131	
MCPF-FCI	−0.001	4.1	−0.043	−0.051
CPF-FCI	−0.002	7.3	−0.047	−0.017
(211)-CAS-FCI	−0.001	−57.2	−0.729	−0.285
(211)-CAS MRCI-FCI	−0.001	+0.4	−0.041	−0.054
(222)-CAS-FCI	+0.007	−33.4	−0.183	−0.008
(222)-CAS MRCI(0.05)-FCI[b]	0.000	0.2	0.000	0.000
(222)-CAS MRCI-FCI	0.000	−1.4	−0.012	−0.001

[a] The full CI values are given explicitly, and all other values are given as differences from the FCI. All configurations in the CASSCF are used as references unless otherwise noted. [b] The reference configurations are chosen with use of a threshold of 0.05.

the errors are still significant. The (211)-CAS result also has a sizeable error, but the DMF is significantly improved with the addition of correlation. When an extra π orbital is added to the active space, the (222)-CAS results are significantly improved and the corresponding MRCI results are in essential agreement with the FCI. By using a threshold of 0.05 in the selection of the references for the MRCI, denoted MRCI(0.05), yields result that are very similar to those obtained by using the full CASSCF space as references. Finally we should note that adding the extra π orbital accounts for the very important p to p′ correlation in O and O^-. However, adding the analogous pσ orbital does not affect the results, and in fact its very low occupation in the CASSCF leads to convergence problems.

Since the (222)-CAS MRCI(0.05) approach essentially reproduces the FCI DMF, the one-particle basis set was calibrated[31] by using this level of n-particle treatment (see Table II). In all calculations the O sp basis is an ANO set developed from the (13s8p) primitive set of van Duijneveldt.[32] This is contracted [5s4p] and then a diffuse s and p function is added. The H ANO basis is (8s6p4d)/[4s3p2d]. As the O sp set and the H basis set are expected to be near the basis set limit for the calculation of the dipole moment, the calibration study focuses on the O polarization functions. We consider both the polarization functions optimized by Dunning[33] for atomic correlation and the ANO basis sets. In the ANO sets the primitive functions of the polarization sets are chosen to cover a wide range of exponents, and they are contracted on the basis of atomic correlation. Thus the two sets of polarization functions are similar in that they are both developed to maximize atomic correlation. The uncontracted Dunning sets might have more flexibility in the outer regions of the wave function; this region is of little importance for atomic correlation, but potentially affects the DMF. Thus more flexible ANO sets are also considered, which have the outermost primitive function uncontracted. We employ the notation [(1 + 1)d] to indicate that there are two

TABLE II. Spectroscopic Constants and Dipole Moments for the $X^2\Pi$ State of OH at the (222)-MRCI Level

basis set[a]	r_e, a_0	D_e, eV	μ_e, au	$d\mu_e/dr$, au/a_0	r^{μ}_{max}, a_0
A. Dunning Polarization Exponents					
(1d)	1.826	4.609	0.6408	0.0930	2.182
(2d)	1.827	4.572	0.6467	0.0988	2.214
(2d1f)	1.835	4.558	0.6505	0.1041	2.248
(3d1f)	1.835	4.561	0.6510	0.1056	2.258
(3d2f)	1.834	4.563	0.6535	0.1066	2.276
(3d2f1g)	1.836	4.584	0.6557	0.1107	2.283
(4d2f1g)[b]	1.836	4.587	0.6466	0.1055	2.290
B. ANO Polarization Exponents					
[1d]	1.825	4.587	0.6412	0.0979	2.205
[2d1f]	1.835	4.562	0.6515	0.1072	2.265
[3d2f1g]	1.837	4.590	0.6548	0.1112	2.293
C. ANO Polarization Exponents with Most Diffuse d Function Uncontracted					
[(1 + 1)d]	1.826	4.571	0.6303	0.0908	2.215
[(1 + 1)d1f]	1.832	4.586	0.6385	0.0970	2.245
[(2 + 1)d1f]	1.835	4.562	0.6416	0.0995	2.270
[(2 + 1)d2f]	1.834	4.568	0.6434	0.1006	2.276
[(2 + 1)d2f1g]	1.837	4.590	0.6464	0.1050	2.293
[(2 + 1)d2f1g][c]	1.836	4.599	0.6451	0.1040	2.296
[(3 + 1)d2f1g]	1.837	4.592	0.6466	0.1058	2.298
[(3 + 1)d2f1g1h]	1.836	4.600	0.6471	0.1060	2.298
(6d4f2g)	1.838	4.589	0.6475	0.1064	2.306
Turnbull[d]			0.6494	0.1298	2.290
expt[e]	1.8342	4.62			

[a] See ref 31 for definition of basis sets. [b] An even-tempered diffuse d function is added to the Dunning (3d2f1g) polarization set for oxygen. [c] A diffuse even-tempered s and p function and an f polarization function are added to the hydrogen basis set. [d] Turnbull and Lowe, ref 38. [e] Huber and Herzberg, ref 34.

d functions, the first is the ANO function while the other corresponds to the outermost primitive uncontracted.

First the results using the successively larger polarization sets of Dunning were considered. These show a relatively smooth convergence to those obtained in the largest (3d2f1g) polarization set. The D_e, for example, first decreases, but then monotonically increases and converges to a value that is 0.04 eV smaller than experiment.[34] We attribute the initial decrease to a reduction in the superposition error.[35] The monotonic increase is due to a systematic reduction in basis set incompleteness. However, the DMFs obtained with the Dunning sets differ from the larger (6d4f2g) primitive set. We attribute this to the lack of a diffuse d function in the Dunning basis set; this is supported by the fact that the addition of a diffuse d function to the Dunning (3d2f1g) set brings the dipole moment into agreement with the larger uncontracted set.

The systematic expansion of the ANO sets leads to results that are very similar to those obtained by using the Dunning sets. That is, the smaller ANO sets lack flexibility in the outermost regions, just like the Dunning sets. Since the primitive polarization functions used in the ANO sets are sufficiently diffuse to describe the outermost regions, the ANO sets are improved by uncontracting the primitive function with the smallest exponent. The systematic expansion of these polarization sets lead to a value in good agreement with the uncontracted polarization set. The inclusion of an h function on O or diffuse s and p functions and an f polarization function of H make very little difference in the dipole moment or its derivative. Therefore, the results are expected to be near the one-particle limit.

TABLE III. Variation of the Spectroscopic Constants and Dipole Moments with the *n*-Particle Treatment[a]

	r_e, a_0	D_e, eV	μ_e, au	$d\mu_e/dr$[b]	r^{μ}_{max}, a_0
[(2 + 1)d2f1g] Oxygen Set					
(2220)-CAS/MRCI (0.05)	1.837	4.592	0.6466	0.1058	2.298
(2220)-CAS/MRCI (0.00)	1.836	4.572	0.6460	0.1041	2.289
(2220)-CAS/MRCI (0.00) field			0.6438	0.1012	2.290
(2220)-CAS/MRCI + Q (0.00) field			0.6457	0.0966	2.291
(3221)-CAS/MRCI (0.01)	1.837	4.576	0.6478	0.1031	2.284
(2220)-CAS/ACPF (0.00)	1.837	4.581	0.6485	0.0996	2.279
(2220)-CAS/ACPF (0.00) field			0.6455	0.0998	2.291
(6d4f2g) Oxygen Set					
(2220)-CAS/MRCI (0.05)	1.838	4.589	0.6475	0.1064	2.306
(2220)-CAS/ACPF (0.00)	1.836	4.593	0.6495	0.1014	2.292
(2220)-CAS/ACPF (0.00) field			0.6466	0.1015	2.306

[a] All calculations employ the [4s3p2d] hydrogen set and the [6s5p] oxygen sp set. [b] Units are au/a_0.

The validity of the procedure of finding a truncated *n*-particle treatment that reproduces the FCI in a basis set of moderate quality, and then taking this approximate *n*-particle treatment to the basis set limit rests on the assumption of no coupling between the one- and *n*-particle treatments. Since it is impossible to carry out FCI calculations in sufficiently large basis sets to assure that no coupling exists, we attempted to assess this by expanding the CASSCF active space and by computing the contribution of higher than double excitations in several ways. The results of these calculations summarized in Table III indicate that the dipole moment and its derivative are relatively unaffected by reference selection, by expanding the CASSCF active space to include a δ orbital, i.e. a (3221)-CAS/MRCI-(0.01) calculation, by computing the dipole moment as an energy derivative instead of as an expectation value, and by the effect of higher than double excitations, as estimated by using either the multireference Davidson correction (+*Q*)[36] or the ACPF method. On the basis of the one- and n-particle calibration studies it is clear that the dipole derivative at r_e must be 0.100 ± 0.005 au/a_0.

In Figure 1 we compare several theoretical DMFs with the empirically determined DMFs of Murphy,[37] Turnbull and Lowe,[38] and Nelson et al.[39] In Figure 1 we have also shown the previous DMF of Werner et al.[40] The theoretical DMFs and that of Murphy have been scaled to reproduce the very accurate experimental values[41] for the dipole moments of $v = 0$ and $v = 1$. It is clear that all of the DMFs, except that of Turnbull and Lowe, are very similar for values of r less than $2.3a_0$. Thus the calculations clearly rule out the DMF of Turnbull and Lowe. The difference between theory and the empirical DMFs at values greater than $2.3a_0$ is a consequence of the fact that the experimental data used to generate the empirical fits does not sample this region of the potential. This is easily demonstrated by computing the percentage of the amplitude of the vibrational wave functions for $r > 2.3a_0$. The results are 0.1, 2.5, 16.6, and 40.7%, for $v = 0$–3, respectively. Thus for the empirical fits to be accurate beyond $2.3a_0$ they must include data from $v = 3$.

The calculations on OH clearly demonstrate that theory can achieve high accuracy for DMFs. By care-

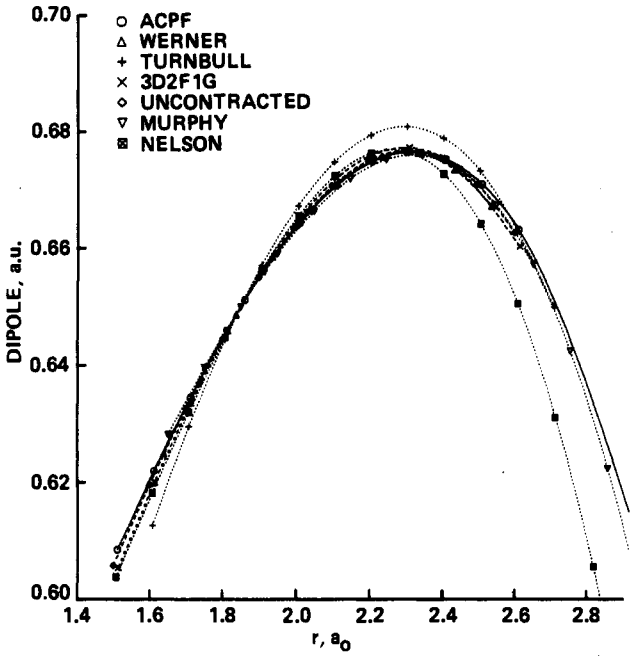

Figure 1. Comparison of several theoretical OH DMFs[31,40] with the empirical DMFs of Murphy,[37] Turnbull and Lowe,[38] and Nelson et al.[39] The theoretical DMFs and the Murphy DMF have been shifted and scaled to reproduce the experimental dipole moments[41] for $v = 0$ and 1. See ref 31 for scale factors (reprinted from ref 31; copyright 1989 American Institute of Physics).

fully calibrating the one and n-particle spaces it is possible to assign very small error bars to the ab initio values. Methods such as CASSCF/MRCI, which reproduce the FCI DMF exceedingly well, are also expected to provide accurate dipole moments for more challenging systems, such as those containing transition metals.

B. Radiative Lifetime of the Vibrational Levels of the $^1\Sigma^+$ State of NO^+

The radiative lifetimes of the individual rovibrational levels are required to determine the energy distribution of vibrationally excited NO^+ produced in the upper ionosphere.[42] The experimental determination of the lifetimes is complicated by the low densities at which ions must be studied. While the experimental measurements of Juo et al.[43] and of Heninger et al.[44] agree with the theoretical results of Werner and Rosmus[45] for $v = 1$, the experimental lifetimes of Kuo et al. fall off much faster with increasing v than the theoretical results. Since the time of the original theoretical work, the accuracy of calculations has improved dramatically. Therefore two theoretical groups[46,47] independently reinvestigated the lifetimes of NO^+, with methods similar to those used for OH. The results of these new theoretical studies are compared with previous results in Table IV. The theoretical results are in excellent mutual agreement, and agree well with the older experimental work of Heninger et al.[44] However, the lifetimes of Kuo et al.[43] for $v > 1$ are substantially smaller. Figure 2 shows the theoretical dipole moments along with a parabolic fit that reproduces the lifetimes of Kuo et al. Clearly the functional form required to reproduce the experimental lifetimes is unreasonable. After the computed results clearly ruled out the recent experimental values, Wyttenbach, Beggs, and Bowers[48] remeasured the lifetimes and found that the original

TABLE IV. Radiative Lifetimes (ms) for the $v = 1$–5 Levels of the $X^1\Sigma^+$ State of NO^+

	theory			experiment			
v	PLB[a]	CR[b]	WR[c]	KBKBL-Z[d]	HFDF-MM[e]	WBB[f]	FHMM-Y[g]
1	90.2	88	91	90 ± 10	95 ± 15	90 ± 10	83
2	46.5	45	48	31^{+6}_{-2}	46 ± 10	49 ± 5	42.5
3	31.9	31	33	16^{+3}_{-1}		30 ± 3	26
4	24.6	24	26			25 ± 3	21.5
5	20.2	20	21			19 ± 3	

[a] Partridge, Langhoff, and Bauschlicher, ref 47. [b] Chambaud and Rosmus, ref 46. [c] Werner and Rosmus, ref 45. [d] Kuo et al., ref 43. [e] Heninger et al., ref 44. [f] Wyttenbach, Beggs, and Bowers, ref 48. [g] Fenistein et al., ref 49; these values contain a 20% uncertainty.

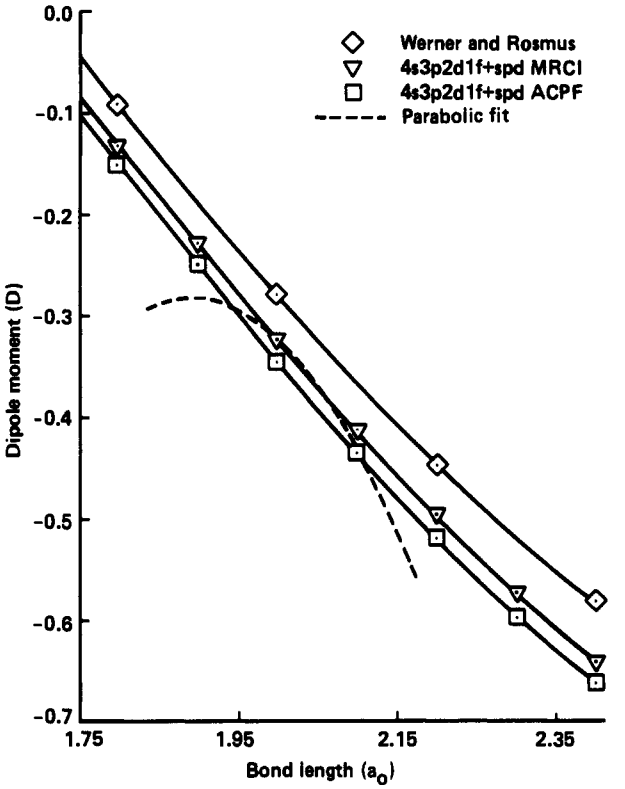

Figure 2. The theoretical NO^+ DMFs determined by Partridge et al.[47] and by Werner and Rosmus[45] and a fitted parabolic DMF (dashed) that reproduces the experimental lifetimes of Kuo et al.[43] (reprinted from ref 47; copyright 1990 North Holand Publishing).

lifetimes were in error due to problems in the ion-excitation process. Their revised experimental values, as well as the very recent work by Fenistein et al.[49] using the monitor ion technique, are in excellent agreement with theory. Thus the theoretical values for higher v are also expected to be accurate and should be adequate for studying the internal energy distribution in NO^+.

C. Triatomic Molecules

Although computationally more expensive than diatomics, many triatomic systems are amenable to accurate theoretical calculations. Not only has there been significant improvement in the quality of ab initio surfaces, but significant progress in solving the triatomic rovibrational problem as well.[50-52] For example, the variational method has now been implemented by using the complete vibration–rotation Hamiltonian for both bent and linear triatomics.[50] Recent advances[51] in

methods of handling large amplitude vibrations such as the discrete variable distributed Gaussian basis method permit the study of highly excited vibrational levels of triatomics, regardless of how floppy they are. For example, it is now possible to study vibrational levels above the HCN/HNC isomerization barrier. Unlike methods based on perturbation theory (vide infra), resonances generally do not present any special problems for variationally based methods.

As an example of state-of-the-art variational calculations on triatomics, we cite the work of Carter and Handy[50] on the rovibrational levels of water. In this work they used a quartic force field derived from spectroscopic data. They computed the vibrational levels up to 12565 cm^{-1} for $J = 0$. Since the agreement with experimentally observed levels was better than 5 cm^{-1}, the theoretical predictions for the energies of five unobserved levels should be accurate as well. They also considered levels with $J \leq 9$ where the agreement with experiment was only slightly poorer. The calculations of the rovibrational levels of H_2O are now sufficiently accurate that theory is not only capable of assigning unidentified lines, but may also be able to contribute to determining the large database of line positions and intensities that are required to define H_2O as an opacity source in stellar atmospheres.

The H_2O study confirms the accuracy and practicality of current methods of solving the rovibrational problem. When experimentally derived force fields are unavailable, it becomes necessary to generate the potential surface by using ab initio methods.[53] For H_2S[53a] the results are also in good agreement with experiment. The errors are slightly larger than for H_2O, because the ab initio potential has greater uncertainty than the experimentally derived quartic potential. However, the results are certainly sufficiently accurate to aid in the identification of the spectra.

To directly compare the computed $\tilde{a}^1A_1$–$\tilde{X}^3B_1$ separation in CH_2 with experiment requires an accurate zero-point energy. Unfortunately only three of the six vibrational frequencies have been measured. By using a completely ab initio approach, the vibrational frequencies of the two states of CH_2 have been computed.[53b] Since the agreement with the three known frequencies is very good and the three remaining frequencies are expected to be of the same accuracy, the zero-point energy should be determined with sufficient accuracy to allow a meaningful comparison of theory and experiment.

We fully expect that many more triatomics will be treated at this level in the near future. Furthermore, accurate solution of the vibrational problem will likely become possible for larger molecules as well. This is important as there are some astrophysical applications where rovibrational spectra of very highly vibrationally excited molecules are required. As experiment is very difficult, we expect theory to contribute substantially to the solution of these problems.

D. Polyatomic Molecules

For polyatomic molecules perturbation theory approaches are commonly used, since a variational solution to the vibrational problem is very difficult. In this subsection we consider these approaches beginning with the double harmonic approximation. In this simplest approach mechanical harmonicity is invoked by describing the vibrational wave functions in terms of harmonic oscillators. Furthermore, the infrared intensity is computed by using only the first derivative of the dipole moment at r_e, which assumes electrical harmonicity. This level of theory is very easy to implement at the SCF level, because efficient methods exist for the analytic evaluation of the second derivatives of the energy with respect to both nuclear motion and other perturbations (e.g., see ref 54). Although the SCF frequencies are generally too large for typical covalent bonds, they tend to be consistently too high and thus amenable to scaling techniques. Since electron correlation generally improves the calculated frequencies, it is noteworthy that efficient analytic techniques for both first and second derivatives for MP2 wave functions have recently been developed.[8] It is also possible to apply the double harmonic approximation to other levels of correlation treatment by using finite difference techniques.

Several examples of the synergism between experiment and theory in solving the vibrational problem have been discussed in a review article by Schaefer.[55] He describes calculations on six ions (H_3O^+, NH_4^+, H_2CN^+, $H_2CO_2^+$, HN_2O^+, and $C_2H_2^+$) where theoretical studies were performed in a sufficiently short time to have a major impact on the experimental studies. For example, theoretical work[56] on H_3O^+ showed that the OH stretch frequency was consistent with the spectra of Saykally and co-workers,[57] thereby differentiating between HO_2^+ and H_3O^+ as potential candidates.

Another example where theory has helped resolve the carrier of a vibrational spectrum involves heavier species.[58] DeVore and Gallaher[59] measured the vibrational frequencies of the reaction products of $TiCl_4$ and NaF. The reaction can yield all products of the form TiF_nCl_{4-n}, for $n = 0,4$. Based on available thermodynamic data they concluded that the only product was TiF_4 and therefore assigned the band at 772 cm^{-1} as the ν_3 mode of TiF_4. The observation of only one mode is consistent with a molecule with T_d symmetry. However, this assignment was shown to be incorrect when the ν_3 band of TiF_4 was later found[60] to lie at 800 cm^{-1}. The results of our theoretical study to determine which specie gave rise to the 772 cm^{-1} band are summarized in Table V. Calculations were carried out at the SCF level, which provides a good description of the wave function, as the bonding is predominantly electrostatic. The SCF vibrational frequencies for both TiF_4 and $TiCl_4$ are in good agreement with experiment and the other TiF_nCl_{4-n} species are expected to be equally well described. The TiF_3Cl and TiF_2Cl_2 species could be ruled out as neither has a frequency near 772 cm^{-1}, and by the fact that there are two strong transitions above 700 cm^{-1}, whereas only one is observed. However, the computed frequency for the Ti–F stretch in $TiFCl_3$ is in excellent agreement with the observed value. In addition, the Ti–Cl stretches are very similar to that in $TiCl_4$, and thus are expected to be obscured by the ν_3 and strong $\nu_1 + \nu_4$ combination bands from unreacted $TiCl_4$. These contentions were subsequently confirmed by an experiment[61] that accounted for the unreacted background $TiCl_4$.

By definition, the double harmonic approximation neglects both the anharmonicity of the potential energy

TABLE V. Summary of TiF_nCl_{4-n} Vibrational Frequencies, in cm^{-1}, and IR Intensities, in km/mol

	TiF_4		TiF_3Cl		TiF_2Cl_2		$TiFCl_3$		$TiCl_4$	
mode[a]	ω_e	I	ω_e	I	ω_e	I	ω_e	I	ω_e	I
ν_2	183 (185[b])	0	155	4	124	2	120	1	113(119[d])	0
	183 (185[b])	0	155	4	153	0	120	1	113 (119[d])	0
ν_4	216 (209[b])	44	203	25	166	17	145	10	140 (139[d])	5
	216 (209[b])	44	203	25	187	15	175	9	140 (139[d])	5
	216 (209[b])	44	204	26	198	17	175	9	140 (139[d])	5
ν_1	712 (712[b])	0	491	135	455	51	424	15	400 (388[d])	0
ν_3	797 (800[c])	320	737	191	525	277	520	250	515 (499[d])	228
	797 (800[c])	320	796	285	758	236	520	250	515 (499[d])	228
	797 (800[c])	320	796	285	795	255	776	231	515 (499[d])	228

[a] Labeled for TiF_4 and $TiCl_4$. [b] Experimental values from Alexander, L. E.; Beattie, I. R. *J. Chem. Soc. Dalton* **1972**, 1972; 1745. [c] Experimental values from ref 60. [d] Experimental values from Hawkins, N. M.; Carpenter, D. R. *J. Chem. Phys.*, **1955**, *23*, 1700.

surface and the fact that the dipole moment is not a linear function of the normal coordinates. To go beyond this approximation[62,63] requires both the energy and dipole moment surfaces to higher order; quartic potentials have generally been used in conjunction with cubic DMFs. It is then possible to use perturbation theory to compute vibrational frequencies that account for anharmonicities and therefore correspond to the experimental fundamentals. By using a quartic force field and cubic dipole moment expansion it is possible to compute the fundamental, overtone, and combination bands and their infrared intensities.

The energies from any level of theory can be used to determine force constants and subsequently the fundamentals for comparison with experiment. Recently the fundamentals of Be_3 and Be_4 have been determined[64] at the coupled cluster level including the effect of triple excitations, CCSD(T).[13] This study indicates the importance of going beyond the double harmonic approximation for these molecules, as the anharmonic correction to the t_2 mode of Be_4 was -111 cm^{-1} or 20%.

The determination of potential surfaces at high levels of theory has been achieved for a few triatomics. For example, a quartic force field for the H_2O molecule has been determined by Bartlett et al.[65] using the CCSDT-1 model[66] and a large Slater basis set. Their harmonic frequencies for the stretching modes were accurate to 3 cm^{-1} and their bending mode was accurate to 28 cm^{-1}. For systems such as Be_n that are not well described by low levels of theory, a high-level treatment of electron correlation may be unavoidable. However, for systems better described by lower levels of theory, we can again take advantage of efficient analytic second derivative methods. Even when analytic techniques are used the calculation of a quartic force field is often expensive, although it can be simplified somewhat by using the observation of Schneider and Thiel[63] that perturbation theory does not require all of the quartic force constants (if normal coordinates are used) and that the required subset can be obtained by central differences of the analytic second derivatives.

The perturbation theory approach has been applied to H_2O at several levels of theory.[62,67] The importance of both anharmonic corrections and correlation were clearly demonstrated;[62] for example, in a DZP basis the effect of correlation on the symmetric O–H stretch fundamental is 269 cm^{-1}, while the anharmonic correction (computed at the MP2 level) is 186 cm^{-1}. At the MP2 level in an extended Gaussian basis set, the fundamentals, overtones, and combination bands are in good agreement with experiment, with errors of less than about 30 cm^{-1}. The fundamental intensities are also in relatively good agreement with experiment, especially considering that even the best experimental intensities are susceptible to systematic errors of 15%. This is a significant improvement over the SCF double harmonic approximation, where the intensities for ν_2 and ν_3 are almost a factor of 2 too large, and ν_1 is almost 1 order of magnitude too large.

An additional approximation that works well is to use a correlated wave function to determine the harmonic force field, but to compute the cubic and quartic terms at the SCF level.[68] This has the advantage that the third derivatives can be computed analytically and the quartic force constants obtained by finite difference techniques. While this method neglects the correlation contribution to the anharmonic correction, it does include the large correlation contribution to the harmonic force field. Since the anharmonic correction is expected to be less than 5%, neglecting the correlation correction to it does not introduce significant error. For H_2O, the anharmonic constants computed in this way[68a] are in error by only about 10%.

This latter approach can be applied to quite large systems. Since the anharmonic corrections are included, the computed results are directly comparable to experiment. Thus, while polyatomic molecules are computationally more difficult, theoretical vibrational frequencies are still sufficiently accurate to aid in interpreting spectra and in determining approximate positions of unobserved bands. An early example of this is the calculation of the vibrational frequencies and intensities of cyclopropenylidene by Lee et al.,[69] which aided in the later identification of this molecule by matrix isolation techniques.[70]

V. Electronic Spectra

The characterization of electronic transitions requires the potential curves for both states and the TMF connecting them. For most approximate wave functions the transition moment is not gauge invariant and thus depends on the representation employed. We defer discussion of the sensitivity of the TM to gauge until Section VC. The TM in the length representation, denoted $D(r)$, for a perpendicular transition (such as $\Sigma^+ \rightarrow \Pi$) is

$$D(r) = \langle \Sigma^+ | (x + iy)/\sqrt{2} | \Pi \rangle \qquad (4)$$

Note that this definition of the matrix element is equivalent to the Cartesian form $\langle \Sigma^+ | x | \Pi_x \rangle$ (Whiting

et al.[71]). However, for all perpendicular transitions not involving a Σ state, the Cartesian form is $\sqrt{2}$ times smaller than that in complex orbitals, e.g.

$$\sqrt{2}\langle \Pi_x|y|\Delta_{xy}\rangle = \left\langle \Pi|(x + iy)/\sqrt{2}|\Delta\right\rangle \quad (5)$$

For parallel transitions the transition moment is, for example,

$$D(r) = \langle \Sigma^+|z|\Sigma^+\rangle \quad (6)$$

To compare with experimental observables such as lifetimes, the transition-moment operator is integrated numerically over the nuclear coordinate r

$$D_{v',v''} = \int_0^\infty \psi_{v'}(r)D(r)\psi_{v''}(r)dr \quad (7)$$

where $\psi_{v'}$ and $\psi_{v''}$ are the upper- and lower-state vibrational wave functions.

Once the dipole matrix element is known, the Einstein A coefficient (s^{-1}) can be obtained as

$$A_{v'v''} = 2.026 \times 10^{-6}\, g\bar{\nu}_{v'v''}{}^3|D_{v'v''}|^2 \quad (8)$$

where $D_{v'v''}$ is in atomic units, $\bar{\nu}_{v'v''}$ is the transition energy in wavenumbers between levels v' and v'' and g is a statistical weighting factor, which is equal to

$$(2 - \delta_{0,\lambda'+\lambda''})/(2 - \delta_{0,\lambda'}) \quad (9)$$

where λ' and λ'' denote the orbital angular momenta of the upper and lower states. The radiative lifetime ($\tau_{v'}$) of a vibrational level depends on the sum of the transition probabilities to all lower vibrational levels in all lower electronic states. If rotational effects are neglected, the lifetime can be written as

$$\tau_{v'} = (\sum_{v''} A_{v'v''})^{-1} \quad (10)$$

A. OH: A Calibration Study of the $A^2\Sigma^+ \rightarrow X^2\Pi$ Ultraviolet System

The hydroxyl radical (OH) is an important component of hydrogen–air mixtures, such as those occurring in hydrogen-burning supersonic combustion ramjets. The $A^2\Sigma^+ \rightarrow X^2\Pi$ line strengths are required to obtain accurate concentration and temperature profiles by using laser excitation fluorescence (LEF) techniques. In addition to combustion processes, the OH radical is a key intermediate in other chemical, atmospheric, and astrophysical systems.

The $A^2\Sigma^+$ state is predissociated by the repulsive $^4\Sigma^-$ state for rovibrational levels above $v' = 1$, $N' = 14$. Therefore, only rovibrational levels below this energy, where the lifetimes are determined solely by radiative decay, are suitable for combustion diagnostics. Unfortunately there is considerable variation in the lifetimes obtained from different experimental techniques. Experiments based on the Hanle effect[72] yield a value of 625 ± 25 ns for $v' = 0$. Use of the high-frequency deflection approach has produced a value of 760 ± 20 ns for OH[73] and 755 ± 40 ns for OD.[74] Lifetimes measured by using the LEF approach have resulted in values of 721 ± 5,[75] 686 ± 14,[76] and 693 ± 10 ns.[77] Theoretical values[78-80] before 1987 are generally in the range 590–636 ns, and thus appear to support the value obtained by using the Hanle effect. This is surprising considering that the more recent LEF measurements are expected to be more accurate. However, none of the previous theoretical studies were sufficiently accurate to rule out any of the experimental determinations.

TABLE VI. Study of the A–X Energy Separation (Δ) and Transition Moment of OH with the Level of Correlation Treatment at $r = 1.80\ a_0$ in the [4s3p2d/2s1p] Gaussian Basis Set

calculation	Δ, cm^{-1} [a]	moment, au
FCI(5)	34 681	0.1010
FCI(7)	33 986	0.1195
SCF	34 850	0.1731
SDCI	34 077 (33 898)	0.1253
MCPF	33 906	0.1214
(222)-CAS	35 372	0.1618
(222)-CAS[b]	36 220	0.1693
(222)-MRCI (0.0)	34 043 (33 876)	0.1230
(222)-MRCI (0.05)	34 131 (33 897)	0.1232
(3221)-CAS	34 609	0.1235
(3221)-MRCI (0.0)	34 013 (33 933)	0.1198
(3221)-MRCI (0.01)	34 033 (33 952)	0.1200
(3221)-MRCI (0.02)	34 002 (33 947)	0.1221

[a] The values in parentheses include the Davidson correction. [b] Separate CASSCF calculations are performed for the two states and a nonorthogonal transition moment is evaluated.

To gain insight into the computational requirements for computing accurate TMFs, a FCI benchmark study of the $A^2\Sigma^+$–$X^2\Pi$ transition in OH was undertaken.[81] A comparison of various approximate correlation methods with the FCI results is given in Table VI. The FCI calculations were performed correlating both five and seven electrons. Although correlation of the oxygen 2s-like orbital changes the separation by only 2%, it increases the transition moment by 20%. Thus seven electrons were correlated in all subsequent calculations. On the basis of the calibration study of the OH dipole moment (vide supra), we consider only two CASSCF active spaces. However, in this case we use a state-averaged approach including the $A^2\Sigma^+$ and $X^2\Pi$ states with equal weights. The (222) active space includes only $p\pi \rightarrow p'\pi$ correlation, while in the larger (3221) active space an oxygen δ orbital is added as well. The A–X separation is remarkably insensitive to the level of treatment. Satisfactory agreement with the FCI is achieved even at the SCF level, and almost perfect agreement with the FCI is obtained at the MRCI level.

In contrast to the energy separation, the A–X transition moment is rather sensitive to the level of theory. The SCF and (222)-CAS TMs are substantially too large. Since the (222)-CAS value increases slightly when separate orbitals are used for each state, it is the lack of correlation and not the state-averaging procedure that causes the large discrepancy with the FCI. Inclusion of correlation in the (222)-based calculations improves the results, but the transition moment is still too large. The MRCI(0.0) calculations (the notation 0.0 denotes no reference selection) show that the error is not associated with selection of reference configurations, but rather that the zeroth-order reference space is too small. Expanding the CASSCF active space to include a δ orbital reduces the CASSCF value such it is comparable to the MRCI value obtained by using the smaller (222) active space. Adding more extensive correlation in the (3221)-MRCI approach yields a transition moment that is in excellent agreement with the FCI, provided the reference threshold is ≤ 0.01. A tighter threshold is required for the (3221)-MRCI cal-

TABLE VII. Study of the OH A-X Energy Separation and Transition Moment with Basis Set Improvement at r = 1.80 a_0

basis set	CI calculation	Δ, cm^{-1}	moment, au
[4s3p2d/2s1p]	(222)-MRCI (0.05)	34 131	0.1232
[4s3p2d/2s1p]	(3221)-MRCI (0.0)	34 013	0.1198
[6s5p4d2f1g/4s3p2d]	(222)-MRCI (0.05)	33 521	0.1316
[6s5p4d2f1g/4s3p2d]	(3221)-MRCI (0.01)	33 385	0.1276
[7s6p4d2f1g/4s3p2d]	(222)-MRCI (0.05)	33 887	0.1320
[7s6p4d3f1g/4s3p2d]	(222)-MRCI (0.05)	33 519	0.1314

TABLE VIII. Summary of the $A^2\Sigma^+$ Lifetimes (ns) of OH

	ref	v' = 0	v' = 1
Theory			
Werner et al. (MCSCF-SCEP)	78	590	643
Langhoff et al. MRCI	79	610	700
Langhoff et al. MRCI	79	580	635
Chu et al. MRCI	80	636	
(3221)MRCI (RKR)	81	669	712
(3221)MRCI (ab initio)	81	672	724
Experiment			
German et al.	72	625 ± 25	
Brzozowski et al.	73	760 ± 20	
Bergeman et al. (OD)	74	755 ± 40	
German	77	693 ± 10	736 ± 11
Dimpfl-Kinsey	76	684 ± 14	
McDermid-Laudenslager	75	721 ± 9	

culation, because most of the configurations involving the δ orbital in the CASSCF have relatively small coefficients.

The FCI benchmark calculations[81] clearly demonstrate that the δ orbital must be included in the CASSCF active space to compute an accurate transition moment. In contrast, the smaller active space is sufficient for computing an accurate DMF.[29] This is not a consequence of the state-averaging procedure, as the dipole moment for the $X^2\Pi$ state in the (222)-MRCI is only increased by 0.2% when the state-averaged CASSCF orbitals are used. The $A^2\Sigma^+$ state dipole moment is also essentially unchanged. Thus an important conclusion of the FCI study is that the n-particle requirements for a transition moment can be more stringent than for either the energy separation or single-state properties.

Our calibration of the one-particle basis set is summarized in Table VII. The smallest basis set considered is the [4s3p2d/2s1p] basis used in the FCI calibration. The next largest set is the [6s5p4d2f1g/4s3p2d] basis that is close to the one-particle limit for the DMF of the $X^2\Pi$ state of OH. Clearly, improving the basis set has a substantial effect on the transition moment. The change in the transition moment between these two basis sets is larger than for the dipole moment. Thus some further studies of the one-particle basis set requirements were undertaken. If the [6s5p4d2f1g/4s3p2d] basis has a limitation, it is probably in the diffuse part of the O s and p space or in the oxygen f primitive set. These potential limitations were addressed by adding a diffuse even-tempered s and p function and by expanding the (4f)/[2f] polarization set to (5f)/[3f]. Since these basis set improvements give small but opposite contributions to the transition moment, the [6s5p4d2f1g/4s3p2d] basis should give results near the basis set limit.

The (3221)-MRCI treatment in the [6s5p4d2f1g/4s3p2d] basis set is expected to yield a TMF very close to the exact one unless there is an unexpected coupling

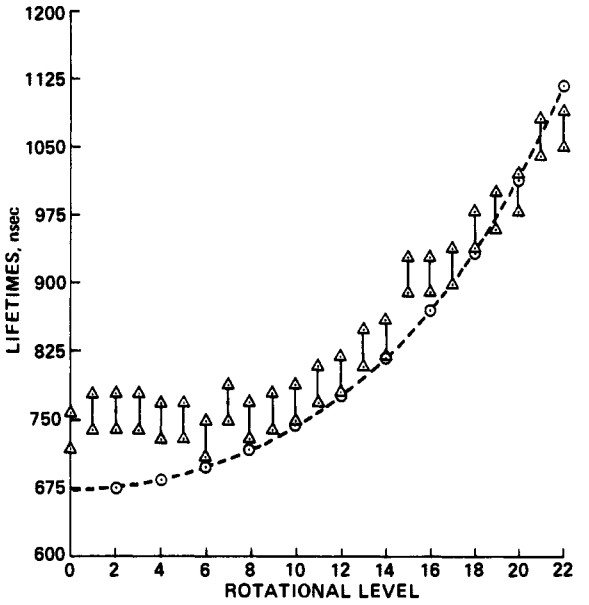

Figure 3. Comparison of the theoretical radiative lifetimes[81] for different rotational levels of the v' = 0 level of the $A^2\Sigma^+$ state of OH (dashed line) with the high frequency deflection measurements (F_1 component) of Brzozowski et al.[73] shown with error bars (reprinted from ref 81; copyright 1987 American Institute of Physics).

between the one- and n-particle spaces. The (3221)-MRCI lifetimes are reported in Table VIII along with the results of previous theory and experiment. The lifetimes are not significantly changed by replacing the theoretical potential by the RKR potential, as expected since the theoretical potential yields vibrational spacings that are in excellent agreement with experiment.[82] The (3221)-MRCI lifetimes are significantly longer than all previous theoretical results. On the basis of the FCI benchmark calculations, this difference largely arises from an improved treatment of the contributions from the oxygen δ orbital.

The (3221)-MRCI lifetimes are expected to be a lower bound, on the basis of the one- and n-particle calibrations, and accurate to about 2%. Thus theory can unambiguously rule out the smaller lifetime value determined by using the Hanle effect and the larger values determined by using the high frequency deflection (HFD) or LEF techniques. Theory is in excellent agreement with the LEF results of German[77] and of Dimpfl and Kinsey.[76] Combining these experimental results with the (3221)-MRCI leads to a recommended value of 685 ± 20 ns for v' = 0 and N' = 0.

While the older value determined from the Hanle effect[72] is, not unexpectedly, slightly low, it is somewhat surprising that the HFD lifetimes[73] for the lowest rovibrational level are significantly too large. In Figure 3 we compare the computed and HFD lifetimes as a function of rotational level. In contrast to the HFD lifetimes, the theoretical values have the expected monotonic increase with N' (due to the nearly linear decrease in the TM with increasing r values). Since the experimental and theoretical lifetimes agree well for larger N', the calculations suggest that there is some systematic error in the HFD lifetimes for small N', possibly due to collisional quenching. In any case we contend that theory is now sufficiently accurate to recommend a lifetime of 685 ± 20 ns for the lowest rovibrational level, thereby allowing us to identify the

TABLE IX. The Difference between the FCI Transition Moments (au) and Those Obtained from Approximate Levels of Correlation Treatment for the $A^1\Pi_u$–$X^1\Sigma_g^+$ Transition in C_2[a]

	r, a_0		
	2.2	2.6	3.0
Two-State Calculations			
MRCI (0.05)	0.005 15	0.008 37	0.040 38
MRCI (0.025)	0.002 83	0.005 74	0.037 79
MRCI (0.01)	0.001 87	0.002 11	0.008 18
MRCI (0.00)	0.000 88	0.000 69	0.002 85
Three-State Calculations			
MRCI (0.05)	0.006 41	0.005 57	0.009 25
MRCI (0.025)	0.004 34	0.003 72	0.002 56
MRCI (0.01)	0.003 40	0.003 00	0.002 61
MRCI (0.00)	0.002 32	0.001 80	0.001 62
FCI	0.344 02	0.280 81	0.148 90

[a] The values are reported as X-FCI so that a positive sign indicates that the MRCI transition moment is larger than the FCI value.

TABLE X. Calibration of the One-Particle Basis Set at r = 2.6 a_0 and a Test of the Coupling of One- and n-Particle Basis Sets for the C_2 $A^1\Pi_u$–$X^1\Sigma_g^+$ Phillips System[a]

treatment	ΔE, cm^{-1}	TM, au
A. [4s3p2d1f]MRCI (0.05)	5494	0.322 66
B. A + uncontracted s and p MRCI (0.05)	5458	0.324 81
C. A + diffuse s and p MRCI (0.05)	5456	0.326 36
D. C MRCI (0.025)	5377	0.298 18
E. C MRCI (0.01)	5380	0.296 46
F. C MRCI (0.01) with δ orbitals	5260	0.296 96
G. C MRCI (0.01) with σ_g, π_u, and δ_g orbitals	5200	0.294 76
H. [7s6p3d2f1g] MRCI (0.025)	5211	0.296 32

[a] In all calculations the reference configurations are chosen on the basis of a two-state CASSCF calculation at r = 2.6 a_0.

correct experimental determination of the lifetime.

B. The Phillips ($A^1\Pi_u$–$X^1\Sigma_g^+$) System of C_2

C_2 is observed in flames and a number of astronomical objects.[83] The absorption lines from the $\Delta v = v' - v'' = -2$ transition of the Phillips system have been used to determine carbon abundances in stellar atmospheres.[84] The Phillips system is important in cold and tenuous interstellar clouds,[85] since the low-temperature conditions prevent absorption from the intense bands originating from the very low-lying $a^3\Pi_u$ state.

The experimental lifetimes of the Phillips system[86-89] have varied by almost a factor of 2. The best results appear to be those of Bauer et al.[86,87] who monitored the emission after laser photolysis. They were able to measure[86] the lifetimes from $v' = 0$ to 8 (higher levels are obscured by the Swan system). Excluding $v' = 0$, their lifetimes showed a monotonic decrease with v'. Since their $v' = 0$ lifetime was potentially affected by emission from the $b^3\Sigma_g^-$ state, they studied[87] this level as well as $v' = 3$ using laser-induced fluorescence (LIF). Their two experimental values for $v' = 3$ agreed, but the new lifetime for $v' = 0$ was longer, so that the experimental lifetimes now decreased monotonically with v'. The theoretical lifetimes[90-93] are mutually consistent, but not in good agreement with the experiments of Bauer et al.[86,87] Given the importance of this system as a carbon-abundance indicator in stars, accurate calculations similar to those for OH were carried out. FCI calculations[93] were again used to calibrate the n-particle treatment (see Table IX). A previous theoretical study[92] indicated that the TMF was affected by the avoided crossing between the $X^2\Sigma^+$ and $(2)^2\Sigma^+$ states at an r value somewhat larger than the Franck–Condon region for the Phillips system. Thus the computed transition moment was sensitive to whether the orbitals were optimized by using an MCSCF procedure that included only the X and A states or the X, A, and $(2)^1\Sigma_g^+$ states. The FCI study showed that at larger r values fewer references are needed in the MRCI if based on the three-state optimization. However, at r values away from the avoided crossing or for very small reference selection thresholds, the number of states included in the CASSCF optimization made only a small difference. Furthermore, the FCI benchmark study showed that the CASSCF/MRCI approach accounts for all of the important correlation effects.

The calibration of the one-particle basis and tests for coupling of one- and n-particle treatments are shown in Table X. The transition moment is increased slightly both by adding diffuse s and p functions and by uncontracting the outermost s and p functions. The results in Table X indicate that a small reference selection threshold is required for accurate results; this is the same conclusion as was drawn from the FCI calibration study. Adding the δ_u and δ_g orbitals or adding the σ_g, π_u, and δ_g components of the C 3d orbital has little effect in C_2. Finally increasing the basis set by adding another s–g ANO makes only a small difference. The calibration study suggests that the computed transition moments (lifetimes) should be accurate to 2% (5%).

TABLE XI. Summary of the Radiative Lifetimes (μs) of the $A^1\Pi_u$ State of C_2

	theory				experiment			
v'	LBRK[a]	ORW[b]	van D[c]	CPB[d]	B85[e]	B86[f]	ELLM[g]	McD[h]
0	13.0	14.1	11.1	10.7	13.4 ± 2.5	18.5 ± 3.0		
1	10.4	11.1	9.0	8.3	15.0 ± 4.0			
2	8.8	9.3	7.6	6.9	14.4 ± 2.0			
3	7.6	8.1	6.6	6.0	12.0 ± 2.0	11.4 ± 2.0	12.1 ± 2.0	
4	6.8	7.2	5.9	5.3	10.7 ± 2.0		11.0 ± 1.1	10.1 ± 1.2
5	6.2	6.5	5.3	4.9	7.9 ± 2.0			
6	5.7	6.0	4.9	4.5	7.0 ± 1.5		10.2 ± 1.3	
7	5.3	5.6	4.6	4.3	6.7 ± 1.0		12.5 ± 1.3	
8	5.0	5.3	4.3	4.0	6.8 ± 1.0			

[a] Theoretical lifetimes of Langhoff, Bauschlicher, Rendell, and Komornicki, ref 93. [b] Theoretical lifetimes of ONeil, Rosmus, and Werner, ref 92. [c] Theoretical lifetimes of van Dishoeck, ref 90. [d] Theoretical lifetimes of Chabalowski, Buenker, and Peyerimhoff, ref 91. [e] Experimental lifetimes of Bauer et al., ref 86, based on time-resolved emissions following laser photolysis of C_2H_2. [f] Experimental lifetimes of Bauer et al., ref 87, based on laser-induced fluorescence studies. [g] Experimental lifetimes of Erman et al., ref 88, using the high frequency detection technique. [h] Experimental lifetimes of McDonald, Baronavski, and Donnelly, ref 89, based on time-resolved emissions following laser photodissociation of C_2H_2.

The computed lifetimes at the MRCI level are compared with previous work in Table XI. The MRCI lifetimes are larger than the older theoretical calculations of van Dishoeck[90] and Chabalowski et al.[91] and slightly smaller than the recent values reported by ONeil et al.[92] The calculations, as well as the experiments of Bauer et al.,[86,87] are inconsistent with the older experimental values of Erman et al.,[88] for the relative lifetimes of $v' = 6$ and 7. The theoretical lifetimes have the same variation with v' as the experimental values of Bauer et al., but are 20% smaller. This difference is well outside the expected accuracy of the theoretical values, which indicates the possibility of some systematic error in the experimental measurements.

C. Gauge Dependence of the Transition Moment

Current state-of-the-art calculations can determine radiative lifetimes to an accuracy of 5% or better for molecules such as OH and C_2. The calibration calculations required to achieve this accuracy are very time-consuming and cannot be carried out for most molecules. Therefore, it is of interest to find a diagnostic of the quality of computed transition moments. Recently we considered[94] whether the difference between the TMs computed from the length and velocity representations constituted a viable diagnostic of the convergence of the wave function. The TM in the length and velocity representations are defined as

$$\langle \Psi_a | \sum_{k=1}^{n} r_k | \Psi_b \rangle \tag{11}$$

and

$$(E_a - E_b)^{-1} \langle \Psi_a | -i \sum_{k=1}^{n} \nabla_k | \Psi_b \rangle \tag{12}$$

respectively, where Ψ_a and E_a are the wave function and energy of state a. We did not consider the acceleration representation

$$(E_a - E_b)^{-3} \langle \Psi_a | -\sum_{k=1}^{n} \nabla_k V | \Psi_b \rangle \tag{13}$$

where V is the potential energy, as this has been shown to be extremely slowly convergent. The TM computed in these three representations will agree for the exact wave function, i.e. a complete configuration–interaction (CI) wave function (FCI in an infinite (complete) one-particle basis) with all electrons correlated. Although previous work has shown[95,96] that the TM in the length representation converges much faster than in the velocity representation, it seemed worthwhile to reconsider this problem by using modern day methodology and FCI calibration calculations.

In our gauge study we considered four transitions in H_2, the $A^1\Pi$–$X^1\Sigma^+$ transition in BH, and the $A^1\Pi_u$–$X^1\Sigma_g^+$ Phillips system of C_2. We consider only the C_2 results here, which are summarized in Table XII. In a small [3s2p1d] basis set, the velocity and length representations differ by more than 25% at the SA-CASSCF level with the $X^1\Sigma^+$ and $A^1\Pi$ states included with equal weights in the averaging. Including 1s correlation leaves the length TM unchanged, but reduces the velocity result by over 15%. The results in the velocity representation are far more sensitive to the reference selection threshold than in the length representation. Expanding the basis set increases the length TM slightly, but dramatically reduces the TM in the velocity representation.

TABLE XII. Comparison of the Length and Velocity Transition Moments for the $A^1\Pi_u$–$X^1\Sigma_g^+$ C_2 Transition

	ΔE, cm^{-1}	TM, au	
		length	velocity
Two-State Calculations			
[3s2p1d] CAS-Ref	6003	0.2768	0.2018
[3s2p1d] CAS-Ref (1s)	6031	0.2766	0.1668
[3s2p1d] MRCI (0.05)	5820	0.3040	0.1077
[3s2p1d] MRCI (0.025)	6048	0.2833	0.2041
[4s3p2d] MRCI (0.025)	5433	0.2966	0.0246
[4s3p(2 + 1)[a]d] MRCI (0.025)	5437	0.2940	0.0091
[4s3p(2 + 1)d] MRCI (0.025)[b]	5427	0.2870	0.0204
[(5 + 1)s(4 + 1)p2d] MRCI (0.025)	5368	0.3007	0.0677
Three-State Calculations[c]			
[3s2p1d] CAS-Ref	5974	0.2777	0.1398
[3s2p1d] CAS-Ref (1s)	6006	0.2777	0.0996
[3s2p1d] MRCI (0.025)	5997	0.2798	0.1099
[4s3p(2 + 1)d] MRCI (0.025)	5366	0.2974	0.1281
[(4 + 1)s(3 + 1)p(2 + 1)d] MRCI (0.025)	5290	0.3013	0.2158
[(4 + 1)s(3 + 1)p(2 + 1)d] MRCI (0.025) (1s)	5375	0.3019	0.2725
[(4 + 1)s(3 + 1)p(2 + 1)d1f] MRCI (0.025)	5328	0.2999	0.1929
[(4 + 1)s(3 + 1)p2d] MRCI (0.025)	5303	0.3005	0.1819
[(4 + 1)s(3 + 1)p(2 + 1)d] + (sp)[d] MRCI (0.025)	5282	0.3016	0.2218
[(5 + 1)s(4 + 1)p3d2f1g] + (sp) MRCI (0.025)	5237	0.2924	0.2530
[(5 + 1)s(4 + 1)p(3 + 1)d2f1g] + (sp) MRCI (0.025)	5236	0.2912	0.2252

[a] Indicates two ANOs with the outermost primitive uncontracted. [b] Three-state reference list. [c] MRCI (0.025) calculations use the 0.025 reference list selected based on r values between 1.8 and 5.0 a_0 from ref 93. [d] Indicates that an even-tempered s and p function have been added.

By using the orbitals from the three-state optimization, involving the $X^1\Sigma_g^+$, $A^1\Pi_u$, and $(2)^1\Sigma_g^+$ states, leads to very different results. The difference between the length and velocity representations is even larger and the velocity representation is more sensitive to the reference selection threshold. Unlike the two-state calculations, improving the basis set increases the velocity TM. Even in the largest basis set the velocity and length TMs differ by 12%. The sensitivity of the velocity TM to level of theoretical treatment is due to the fact that the TM derives from a cancellation of many large contributions of opposite sign. In addition, the calculations show that the TM in the velocity representation is sensitive to core correlation while the length TM is not. The difference between the velocity and length TMs does not appear to be correlated with the accuracy of the length TM. Even with the highest levels of theory available today, the difference between the length and velocity TMs does not appear to be a viable diagnostic of the quality of molecular wave functions. Thus we feel that the best approach for determining the reliability of a TMF is to study its sensitivity to a systematic variation of the one- and n-particle treatments in the length representation.

D. Identification of the Hermann Infrared System of N_2

The Hermann infrared system (HIR) consists of a group of multiheaded bands in the region 700–970 nm. This band system was observed in 1951 by Hermann[97] in a low current discharge through pure N_2 at low temperature. Later Carroll and Sayers[98] were able to show that the bands must result from either a triplet or quintet transition. More recently Nadler et al.[99–101] demonstrated that the HIR system was generated by

TABLE XIII. Comparison of Theoretical Vibrational Levels (cm^{-1}) of the $A'^5\Sigma_g^+$ and $C''^5\Pi_u$ States of N_2 with Those Deduced from the HIR Bands

level	$A'^5\Sigma_g^+$		$C''^5\Pi_u$	
v	theory	HIR bands	theory	HIR bands
0	352.3	352.3[a]	451.3	451.3[a]
1	1054.7	1067.3	1325.6	1337.3
2	1725.6	1741.3	2167.0	2200.5
3	2346.2	2376.8	2989.7	3036.9
4	2916.4	2988.3	3787.8	
5	3417.9		4564.4	
6	(3813.0)		5354.6	

[a] The energy of the $v = 0$ levels were set equal to theory; the actual values may be slightly larger. The remaining energies were obtained by taking the averages of the appropriate band origin differences for the observed bands. The experimental values are deduced from ref 101.

the energy pooling reaction between metastable N_2 ($A^3\Sigma_u^+$) molecules; i.e.

$$N_2\,(A,v=0) + N_2\,(A,v=0) \rightarrow N_2\,(HIR,\ v = 3) + N_2\,(X,v') \quad (14)$$

Although v' was not known, this required that the energy of HIR upper state be less than 12.02 eV above the ground state. Furthermore, the positions of the $v' = 0$–3 and $v'' = 0$–4 were known as were the relative intensities. Based on this Nadler and Rosenwaks[101] suggested that the HIR system might originate from the unobserved $(II)^3\Pi_u$ state to the $G^3\Delta_g$ state. They ruled out a possible identification with the $C''^5\Pi_u \rightarrow A'^5\Sigma_g^+$ transition, since existing estimates of the well depth of the A′ state were inconsistent with the observation of four vibrational levels.

Recently we studied[102] the Lewis–Rayleigh afterglow of N_2 to elucidate the population mechanism for the $B^3\Pi_g$ state. Since one of the two competing population mechanisms involved the $A'^5\Sigma_g^+$ state, an accurate potential was determined. The resulting $A'^5\Sigma_g^+$ potential had a well depth of at least 3450 cm^{-1} and a barrier of about 500 cm^{-1}, whereas previous theoretical estimates[103] of the well depth were around 850 cm^{-1}. The new potential supported six bound and one quasibound vibrational levels. Clearly, this deeper well removes the main objection to the C″ → A′ transition as the carrier of the HIR bands. To investigate this we carried out comparable calculations for the C″ state.

The computed vibrational levels for the A′ and C″ states are compared with those deduced from the observed HIR bands in Table XIII. The agreement is excellent, except that the theoretical spacings are slightly smaller, which suggests that the true well depths are, not unexpectedly, slightly larger. The most compelling evidence supporting the assignment of the $C''^5\Pi_u \rightarrow A'^5\Sigma_g^+$ transition to the HIR system is shown in Table XIV where the theoretical 0–0 transition has been shifted by 559 cm^{-1} to agree with experiment.[101] The band positions are clearly very good. Even the relative intensities can be brought into agreement with experiment by assuming that the relative populations for v' = 0–3 are 0.073, 0.295, 1.000, and 0.725, respectively. On the basis of these theoretical results, the HIR system was assigned to the $C''^5\Pi_u \rightarrow A'^5\Sigma_g^+$ transition. Huber and Vervloet[104] have confirmed this assignment spectroscopically, by exciting the emission in a supersonic jet discharge to avoid overlapping bands from the strong first positive system of N_2.

TABLE XIV. Band Positions and Relative Intensities of the HIR System of N_2

band	band positions, nm		relative intensities	
	theory	experiment	theory	experiment
0–0	806[a]	806	3.5	4.0
0–1	854	855	1.0[b]	1.0
0–2	906	907	0.6	
0–3	960	963	0.3	
0–4	1016	1023	0.1	
1–0	753	752	6.0[b]	6.0
1–1	795	795	0.2	
1–2	840	840	0.7	<0.5
1–3	885	887	1.6	
1–4	932	938	1.4	
2–0	707	706	10.0[b]	10.0
2–1	745	744	8.8	8.0
2–2	783	783	6.6	5.0
2–3	823	824	0.3	<0.5
2–4	864	868	0.7	
3–0	668	667	1.5[b]	1.5
3–1	701	700	10.4	9.0
2–3	735	735	0.6	<0.5
3–3	771	771	4.8	3.0
3–4	806	809	2.5	

[a] The 0–0 bands were shifted into coincidence; this required a shift of 567 cm^{-1} in the theoretical T_e. [b] These bands were normalized to experiment by adjusting the vibrational populations. This requires that the relative populations of $v' = 0$–3 be 0.073, 0.295, 1.00, and 0.725, respectively.

E. Al_2

In previous discussion we have focused on the accurate calculation of selected transitions. However, to aid in the identification of experimental spectra, it is often necessary to consider all dipole-allowed transitions below a specified energy. In this subsection we consider Al_2, where many transitions result in a complex spectrum that is difficult to interpret.

Al atom has a $^2P(3s^23p^1)$ ground state. Three candidates for the ground state of Al_2 had been proposed, the $^3\Sigma_g^-(\pi_u^2)$ and $^3\Pi_u(\sigma_g^1\pi_u^1)$ states with two one-electron bonds and the $^1\Sigma_g^+(\sigma_g^2)$ state with one two-electron bond. Previous calculations[105,106] ruled out $^1\Sigma_g^+$ state as the ground state, but the two triplet states were so close in energy that calculations could not resolve which was the ground state. Recently, however, very accurate calculations[107] calibrated against FCI were able to definitively demonstrate a $^3\Pi_u$ ground state.

Recent experiments[108,109] have confirmed that Al_2 has a $^3\Pi_u$ ground state and have identified several new band systems. To aid in the assignment of the spectra, CASSCF/MRCI calculations[110] were carried out for the 12 triplet and six singlet states that lie below about 30 000 cm^{-1}. As the singlet manifold contributes little to spectra, we do not consider it here. The potential curves for the triplet states are plotted in Figure 4 and the spectroscopic constants are summarized in Table XV. As discussed by Langhoff and Bauschlicher[110] and by Fu et al.,[108] these computed potentials are able to explain most of the experimental observations.

The calculations are in good agreement with the well characterized $^3\Sigma_u^- \rightarrow {}^3\Sigma_g^-$ emission system of Al_2.[111] The T_e value, the ω_e values, and the change in bond length between the two states agree well with experiment. The calculations show that the $(1)^3\Pi_g$–$X^3\Pi_u$ transition leads to the broad structureless feature in the region of 15 000 cm^{-1} that was observed in a krypton matrix by Douglas et al.[112] The avoided crossing between the $(2)^3\Pi_g$ and

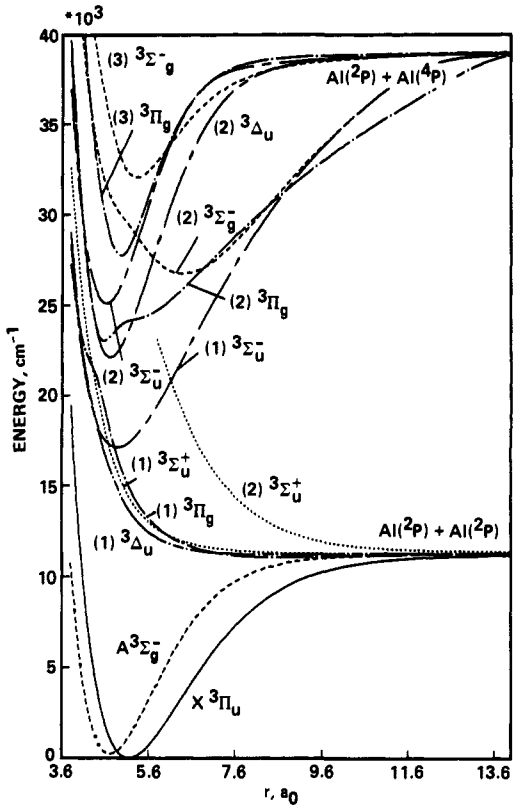

Figure 4. CASSCF/MRCI potential energy curves for the triplet states of Al_2. The symmetries are differentiated by the various types of chained lines (reprinted from ref 110; copyright 1990 American Institute of Physics).

TABLE XV. Summary of CASSCF/MRCI Spectroscopic Constants for Al_2

state	r_e, Å	ω_e, cm^{-1}	T_e, cm^{-1}
$(1)^1\Sigma_u^+$	2.726	256	27838
$(1)^1\Delta_u$	2.695	287	22782
$d^1\Sigma_g^+$	2.738	276	7182
$c^1\Delta_g$	2.561	288	3503
$b^1\Pi_u$	2.746	265	3343
$a^1\Sigma_g^+$	2.955	212	2547
$(3)^3\Sigma_g^-$	2.825	317	32041
$(3)^3\Pi_g$	2.629	495	27749
$(2)^3\Sigma_g^-$	3.226	238	26717
$(2)^3\Sigma_u^-$	2.451	441	25102
$(2)^3\Pi_g$	2.440	490	23054
$(2)^3\Delta_u$	2.498	432	22126
$(1)^3\Sigma_u^-$	2.586	282	17120
$(1)^3\Pi_g$			14927
$(1)^3\Sigma_u^+$			14371
$(1)^3\Delta_u$			13651
$A^3\Sigma_g^+$	2.496	331	227
$X^3\Pi_u$	2.835	274	0

$(1)^3\Pi_g$ states leads to an asymmetric potential for the $(2)^3\Pi_g$ state, which explains the large variation in the ΔG values observed in the absorption experiments of Douglas et al.[112] and Abe and Kolb.[113] Fu et al.[108] suggest that the reason the $(2)^3\Pi_g$–$X^3\Pi_u$ transition has not been observed in emission is because the avoided crossing results in a coupling between the two $^3\Pi_g$ states that leads to rapid predissociation.

The calculations show that the $^3\Sigma_g$ state first observed by Cai et al.[109] is the $(2)^3\Sigma_g^-$ state. Fu et al.[108] suggest that the avoided crossing found in the theoretical potentials between the $(2)^3\Sigma_g^-$ and $(3)^3\Sigma_g^-$ states explains the anomalous intensity patterns observed in the $(2)^3\Sigma_g^-$–$^3\Pi_u$ band system. Fu et al.[108] observed a second more intense transition within the spectral range of the $(2)^3\Sigma_g^-$–$^3\Pi_u$ band system. This system has been assigned to the $(3)^3\Pi_g$–$X^3\Pi_u$ transition on the basis of the T_e value for the $(3)^3\Pi_g$ state and the fact that theory predicts this to be the most intense system below 30000 cm^{-1}. Furthermore, Cai et al. and Fu et al. observed a state at 32636 cm^{-1}, which was tentatively assigned as $^3\Sigma_g$. Although the calculations suggest that the upper state is $(3)^3\Sigma_g^-$, the theoretical results are not sufficiently accurate to make a definitive assignment. In any case it is clear that theory can contribute substantially to interpreting experimental spectra, as a combination of theory and experiment has led to an excellent understanding of the low-lying states of Al_2.

F. Spectroscopy of ZrO

Transition-metal containing compounds are often difficult to study spectroscopically. Theoretical calculations can also be difficult as a result of the mixed bonding that occurs from the d^ns^2, $d^{n+1}s^1$, and d^{n+2} metal occupations. Errors in positioning these asymptotes can result in both an incorrect description of their mixing in a molecule and in incorrectly positioning molecular states derived from different asymptotes. The result is that very high levels of theory are required to study transition-metal systems.[114] The requirements for the calculation of dipole moments are described in ref 115, and the electronic spectroscopy of the transition-metal hydrides has been recently reviewed.[116] In this subsection we consider the spectroscopy of ZrO as a representative example of transition-metal-containing compounds.

ZrO has been observed in S stars,[117,118] but the lack of experimental data for the electronic transition probabilities has prevented ZrO from being included as an opacity source in models of stellar atmospheres. Recently the lifetimes of three transitions in ZrO have been determined spectroscopically.[119,120] Other low-lying states are known,[121-123] but their lifetimes have not been determined and the existence of other low-lying states is expected based on simple molecular orbital arguments. Theory can be used to study these states, and the three known lifetimes can serve as calibration.

The $X^1\Sigma^+$ ground state of ZrO is derived from the $^3F(4d^25s^2)$ ground state of Zr atom and involves the formation of two 4d–2p bonds with O. The 5s electrons polarize away from the oxygen by mixing in $5p\sigma$ character. The excited singlet states are produced by exciting the 5s electrons into the 4d or 5p orbitals. ZrO has a low-lying (T_e = 1487 cm^{-1})$^3\Delta$ excited state[121] that is derived from the $^5F(4d^35s^1)$ excited state of Zr atom. This state is analogous to the $X^1\Sigma^+$ state in that the bonding involves 4d–2p bonds and the 5s orbital is polarized away from oxygen. The excited triplet states are formed by exciting either the 5s or $4d\delta$ electrons.

We have studied[124] the six lowest singlet and triplet states by using the CASSCF/MRCI approach; this accounts for all states below about 23000 cm^{-1}. The active space included the Zr 4d and 5s and O 2p orbitals and electrons. In addition, it was necessary to include an extra π orbital in the active space to properly describe the excited states that have the Zr $5p\pi$ orbital occupied.

The spectroscopic constants for these states are summarized in Table XVI. While some of the MRCI bond lengths are longer and some shorter than exper-

TABLE XVI. Spectroscopic Constants for the Low-Lying States of ZrO

	MRCI			MRCI+Q			expt[a]		
state	r_e, a_0	ω_e, cm^{-1}	T_e, cm^{-1}	r_e, a_0	ω_e, cm^{-1}	T_e, cm^{-1}	r_e, a_0	ω_e, cm^{-1}	T_e, cm^{-1} [b]
$X^1\Sigma^+$	3.253	979.1	0	3.277	941.5	0	3.234	969.8	0
$A^1\Delta$	3.286	940.9	5111	3.302	920.4	5230	3.262	938.1	5904[c]
$B^1\Pi$	3.319	899.9	15168	3.353	857.5	15048	3.323	859.0	15443
$C^1\Sigma^+$	3.325	903.6	17625	3.349	873.2	17278			17099[d]
$D^1\Gamma$	3.318	907.3	17922	3.343	876.4	17530			
$E^1\Phi$	3.303	908.4	23214	3.322	876.2	22415			
$a^3\Delta$	3.283	957.7	953	3.305	926.8	1268	3.266	936.5	1487[e]
$b^3\Pi$	3.301	905.1	12122	3.329	873.9	11566			12249[f]
$c^3\Sigma^-$	3.316	926.3	14427	3.348	879.3	13661			
$d^3\Phi$	3.305	893.1	19010	3.332	864.7	18195	3.309	853.9	17296
$e^3\Pi$	3.314	885.6	21488	3.341	857.4	20353	3.318	845.4	19207
$f^3\Delta$	3.370	847.3	21683	3.399	803.2	21869	3.356	820.6	22031

[a] The spectroscopic constants are taken from Huber and Herzberg[34] unless noted otherwise. [b] The weighted average of fine structure levels. [c] Hammer, Davis, and Zook, ref 122. [d] The 0–0 band was observed at 5860 Å by Simard et al.[120] This was converted to a T_e value by using the MRCI+Q ω_e values. [e] Hammer and Davis, ref 121. [f] Phillips, Davis, and Galehouse, ref 123.

TABLE XVII. Radiative Lifetimes for the Low-Lying States of ZrO

	lifetime ($v' = 0$)		
state	theory	expt	dominant transition
$b^3\Pi$	1.07 μs		$b^3\Pi$–$a^3\Delta$
$d^3\Phi$	45.9 ns		$d^3\Phi$–$a^3\Delta$
$e^3\Pi$	24.4 ns	32.5 ± 2 ns[a]	$e^3\Pi$–$a^3\Delta$
$f^3\Delta$	28.3 ns		$f^3\Delta$–$a^3\Delta$
$B^1\Pi$	56.4 ns	83 ns[b]	$B^1\Pi$–$X^1\Sigma^+$
$C^1\Sigma^+$	136 ns	126 ± 9 ns[b]	$C^1\Sigma^+$–$X^1\Sigma^+$
$E^1\Phi$	30.8 ns		$E^1\Phi$–$A^1\Delta$

[a] The experimental value for $v' = 0$, $J' = 77$ from Hammer and Davis, ref 119. The theoretical value for $J' = 77$ is 25.1 ns. [b] The experimental values for $v' = 0$, from Simard et al., ref 120.

iment, the MRCI+Q values are uniformly $0.03a_0$ too long, probably as a result of neglecting inner-shell (4s4p) correlation. On average, the +Q correction improves the ω_e and T_e values. However, the accuracy is lower than that obtained for first-row systems. For example, the errors in the T_e values of OH and C_2 are 200 and 40 cm^{-1}, respectively, whereas for ZrO the largest error is about 900 cm^{-1}. As the transition moment changes by only a small amount between the CASSCF and MRCI levels, the large transition moments are expected to be accurate to about 10%. While the uncertainties are much greater than the 2% accuracy obtainable for many first-row systems, the theoretical values are still sufficiently accurate to complement experiment.

The radiative lifetimes for the low-lying states of ZrO are summarized in Table XVII. The lifetime of the $C^1\Sigma^+$ state is in excellent agreement with experiment,[120] while the calculated lifetimes of the $B^1\Pi$ and $e^3\Pi$ states are about 25–35% less than experiment.[119,120] The calculated $B^1\Pi$ state lifetimes increase slowly with v' as observed in experiment.[120] Since the computed lifetimes are expected to be accurate to about 20%, the experimental values are not far outside the expected accuracy of the theoretical study. The calculations predict that the $E^1\Phi$–$A^1\Delta$ transition should occur in the same spectral region as the $d^3\Phi$–$a^3\Delta(\gamma)$ transition, which might explain why the calculated transition moment for the γ system is much weaker than that deduced from experiment.[118] Further experimental studies of ZrO, particularly in absorption, would be very worthwhile.

The ZrO study shows that in spite of the great advances in ab initio methods in the last few years, calculations on transition-metal-containing systems are still very challenging. However, even with 1000 cm^{-1} accuracy for the T_e values and 20% uncertainty in the lifetimes, theory can still aid experimental interpretation, considering that the spectra of transition-metal-containing compounds are often extremely complex due to the large number of overlapping lines and large spin–orbit and hyperfine effects.

G. The Complete Active Space State Interaction Approach to Spectroscopy

Up to this point our final wave functions have been generated by using the MRCI approach. For the $A^2\Sigma^+$–$X^2\Pi$ transition in OH, the agreement between the CASSCF and MRCI TMs dramatically improved as the size of the CASSCF active space increased. Therefore, if a sufficiently large active space is used, it may not be necessary to include more extensive correlation using the MRCI approach. This contention is supported by the study of the lifetimes of the $A^1\Pi$ and $C^1\Sigma^+$ states of AlH, where the CASSCF lifetimes[125] are in excellent agreement with the CASSCF/MRCI values[126] and experiment.[127] As expected, in the CASSCF-only study the active space had to be larger than that in the CASSCF/MRCI treatment. One advantage of the CASSCF-only approach is that different orbitals can be used for each state. In those cases where the orbitals are very different for each state a much smaller active space can be used in an individual state optimization than in a state-averaged calculation. This could be quite important in the study of the excited states of aromatic systems, which generally have states of different character, such as covalent, ionic, mixed valence and Rydberg, and those with strong configurational mixing.[128] Clearly, when a common molecular orbital basis is used, a very large active space is required to describe these states of different character equivalently. Large active spaces generally lead to MRCI expansions of prohibitive length. While it is well known that separate CASSCF calculations for each state can yield a much more compact description of the wave functions, the calculation of the transition moment for wave functions with different orbitals, i.e., a nonorthogonal transition moment, was very time consuming. However, Malmqvist[17] showed that for some classes of wave functions this time-consuming bottleneck can be totally eliminated.

If more than one state of the same symmetry is studied, the states are not necessarily orthogonal and noninteracting. By computing both the one- and two-

electron transition density matrices, the overlap and interaction matrix for all states of the same symmetry can be computed. A set of orthogonal noninteracting states can be produced by solving a small secular problem. This procedure, termed the complete active space state interaction (CASSI) method,[129] has been shown to be quite efficient; matrix elements between CASSCF wave functions of a few hundred thousand configurations can easily be computed. Eliminating the contamination by the lower states can have a pronounced effect on the transition moment. For example, in pyrimidine the TM was reduced by about 60% when the contamination was removed.[129]

The CASSI approach was applied in a recent study of the spectroscopy of the nucleic acid base monomers.[128] For cytosine Fülscher et al. performed four SA-CASSCF calculations. The 17 CASSCF wave functions from these SA-CASSCF calculations were used as the basis in the CASSI calculation. The results were shown to be in good agreement with experiment for the transition moment and polarization angle. The excitation energies were in only qualitative agreement with experiment. Much of this error was due to the neglect of $\sigma-\pi$ correlation. It was neglected since the size of the CASSCF expansion grows very rapidly with the number of electrons and orbitals. The restricted active space SCF (RASSCF) approach[16] in which the active space is divided into three parts (in part 1 the orbitals are allowed to have only n holes, part 2 is analogous to the CASSCF active space, and part 3 is allowed to have m electrons) should allow even more accurate treatments.

The CASSI method has a lot of promise for systems with many electrons and states with very different orbital character. In these cases it is likely that the MRCI approach will become intractable. We expect to see many important applications of this method to the excited states of large organic molecules. It is also interesting to note that it might be possible to study transition-metal systems by performing separate calculations for the states arising from the $d^n s^2$, $d^{n+1}s^1$, and d^{n+2} occupations, and then compute the interaction between them using the CASSI method.

H. Spin-Forbidden Transitions in O_2

Up to this point we have discussed only spin-allowed dipole transitions, but spin–orbit coupling induces spin-forbidden transitions by mixing states of different spin. This mixing can substantially affect the spectroscopy of molecules containing heavier elements. Except for very heavy systems, L and S remain good quantum numbers, so that the mixing of these wave functions can be described in LS coupling through the inclusion of the spin–orbit operator. An example is the alkaline-earth atoms where the lifetime of the ^3P state is determined by borrowing intensity from the strong $^1P-^1S$ transition.[130] The $^3P-^1S$ transition is generally referred to as a spin-forbidden dipole-allowed transition. In cases where there are no dipole-allowed transitions, the lifetime will often be determined by magnetic-dipole and electric-quadrupole transitions. Such is the case of the $b^1\Sigma_g^+$ and $a^1\Delta_g$ states of O_2, which we now consider in some detail.

A theoretical study of the lifetimes of the $b^1\Sigma_g^+$ and $a^1\Delta_g$ states of O_2 has been carried out by Klotz et al.[131]

TABLE XVIII. Contributions to the Lifetimes of the $a^1\Delta_g$ and $b^1\Sigma_g^+$ States of O_2[a]

transition	lifetime, s	dominant term
	$b^1\Sigma_g^+$ State	
$b^1\Sigma_g^+ \rightarrow X^3\Sigma_g^- (m_s = 0)$	6.5×10^6	difference in X and b state quadrupole moments
$b^1\Sigma_g^+ \rightarrow X^3\Sigma_g^- (m_s = \pm 1)$	11.65	magnetic dipole
$b^1\Sigma_g^+ \rightarrow a^1\Delta_g$	720	electric quadrupole
	$a^1\Delta_g$ State	
$a^1\Delta_g \rightarrow X^3\Sigma_g^- (m_s = 0)$	5×10^7	electric quadrupole
$a^1\Delta_g \rightarrow X^3\Sigma_g^- (m_s = \pm 1)$	5270	magnetic dipole

[a] These results are taken from ref 131.

They first determined wave functions, ϕ_m, for the $a^1\Delta_g$, $b^1\Sigma_g^+$, $X^3\Sigma^-$, two $^1\Pi_g$, and two $^3\Pi_g$ states using the standard MRCI approach. The effect of spin–orbit coupling is included by using perturbation theory, such that the perturbed wave function, Φ_m, is written in terms of the unperturbed wave functions ϕ_m as

$$\Phi_m = \phi_m + \sum_{k \neq m} a_k \phi_k \tag{15}$$

with the coefficients a_k evaluated as

$$a_k = \langle \phi_k | H_{so} | \phi_m \rangle / (e_m - e_k) \tag{16}$$

where e_k is the energy of state k and H_{so} is

$$H_{so} = \sum_{i,\alpha} \frac{Z_\alpha}{r_{i\alpha}^3} (\mathbf{r}_{i\alpha} \times \mathbf{p}_i)\mathbf{s}_i + \sum_{i,j \neq i} \frac{1}{r_{ij}^3} ((2\mathbf{p}_i - \mathbf{p}_j) \times \mathbf{r}_{ij})\mathbf{s}_j \tag{17}$$

While Klotz et al.[131] determined two $^1\Pi_g$ and $^3\Pi_g$ states, they only included the upper valence state in the calculation of the perturbed wave functions. The lower states are Rydberg in character and therefore were not expected to interact strongly with the valence states.

By using these perturbed wave functions, the lifetimes of the a and b states can be expressed as a linear combination of five spin-allowed transitions which are summarized in Table XVIII. It is clear that the dominant mechanism for both states is magnetic dipole. The computed value of 11.65 s for the b state lifetime is in excellent agreement with the experimental value of 12 s.[132] In addition, the absolute b → a transition probability has been determined to be 2.5×10^{-3} s^{-1} with an uncertainty of a factor of 2.[133] The computed value[131] of 1.4×10^{-3} s^{-1} therefore agrees with experiment to within its stated error bars.

The computed lifetime[131] for the $a^1\Delta_g$ state of 5270 s is within the range of experimental values (3890–6660 s).[34,132] The reliability of the theoretical treatment depends on the convergence of the perturbation series, and in this work only one $^1\Pi_g$ and one $^3\Pi_g$ state were included in the calculation of the perturbed states. This approximation can be circumvented by employing the technique of Yarkony and co-workers,[134-136] which accounts for the mixing of all states of a given symmetry without first determining all LS states. This approach is expected to allow even more accurate treatments of spin-forbidden transitions.

While there have not been many studies of spin-forbidden processes, this should become more commonplace in the next few years. This will allow the treatment of heavier systems. However, to treat very

heavy systems it will be necessary to use methods that do not include spin–orbit effects by perturbation theory, but instead include these terms explicitly in the Hamiltonian. This has been implemented within the conventional CI approach,[137,138] which necessarily restricts the number of configurations that can be considered. Recently this has been implemented[139] within the direct CI approach which will allow much larger CI expansions including spin–orbit effects.

VI. Conclusions

In this review we have given a few examples of the kinds of spectroscopic problems that can be solved with current theoretical methods. The accuracy of approximate methods for including electron correlation have been calibrated by comparison with FCI calculations. The SA-CASSCF/MRCI method is shown to provide an excellent approach for treating several electronic states accurately in a common molecular orbital basis. At the CASSCF/MRCI level it is possible to compute a very accurate transition moment function if care is taken to ensure that the TMF is converged with respect to expansion of the one-particle basis set. For first-row systems such as OH, radiative lifetimes of electronic states can be computed to an accuracy of better than 5%, which allows for a critical assessment of the available experimental data. Theoretical calculations have also been very useful is determining the ground state of molecules and in assigning band systems, such as the HIR band system of N_2. In several cases, theoretical solutions to spectroscopic problems were later confirmed by experiment.

In this review we have been able to illustrate the potential of theory for solving spectroscopic problems. Further advances in the solution of the polyatomic vibrational problem as well as the development of efficient analytic deviative methods for higher levels of correlation treatment should greatly increase the capability of theory in the next few years. Methods for treating spin-forbidden and nonradiative processes are also becoming more efficient and accurate. Therefore we expect that in the future theory will be able to contribute increasingly to the solution of spectroscopic problems.

VII. References

(1) Marian, C. M.; Marian, R.; Peyerimhoff, S. D.; Hess, B. A.; Buenker, R. J.; Seger, G. *Mol. Phys.* **1982**, *46*, 779.
(2) Lengsfield, B. H.; Saxe, P.; Yarkony, D. R. *J. Chem. Phys.* **1984**, *81*, 4549.
(3) Saxe, P.; Lengsfield, B. H.; Yarkony, D. R. *Chem. Phys. Lett.* **1985**, *113*, 159.
(4) *Advances in Chemical Physics: Ab initio methods in quantum chemistry*; Wiley, New York, 1987; Vol. 67 and 69.
(5) Bauschlicher, C. W.; Langhoff, S. R.; Taylor, P. R. *Adv. Chem. Phys.* **1990**, *77*, 103.
(6) Almlöf, J.; Taylor, P. R. *J. Chem. Phys.* **1987**, *86*, 4070.
(7) Pople, J. A.; Binkley, J. S.; Seeger, R. *Intern. J. Quantum Chem. Symp.* **1976**, *10*, 1.
(8) Handy, N. C.; Amos, R. D.; Gaw, J. F.; Rice, J. E.; Simandiras, E. D. *Chem. Phys. Lett.* **1985**, *120*, 151.
(9) Bartlett, R. J. *Ann. Rev. Phys. Chem.* **1981**, *32*, 359.
(10) Ahlrichs, R.; Scharf, P.; Ehrhardt, C. *J. Chem. Phys.* **1985**, *82*, 890.
(11) Chong, D. P.; Langhoff, S. R. *J. Chem. Phys.* **1986**, *84*, 5606.
(12) Urban, M.; Noga, J.; Cole, S. J.; Bartlett, R. J. *J. Chem. Phys.* **1985**, *83*, 4041.
(13) Raghavachari, K.; Trucks, G. W.; Pople, J. A.; Head-Gordon, M. *Chem. Phys. Lett.* **1989**, *157*, 479.
(14) Malmqvist, P.-Å.; Rendell, A.; Roos, B. O. *J. Chem. Phys.* **1990**, *94*, 5477.
(15) Werner, H.-J.; Knowles, P. J. *J. Chem. Phys.* **1985**, *82*, 5053.
(16) Olsen, J.; Roos, B. O.; Jørgensen, P.; Jensen, H. J. Aa. *J. Chem. Phys.* **1988**, *89*, 2185.
(17) Malmqvist, P. A. *Intern. J. Quantum Chem.* **1986**, *30*, 479.
(18) Gdanitz, R. J.; Ahlrichs, R. *Chem. Phys. Lett.* **1988**, *143*, 413.
(19) Shavitt, I. In *Methods of Electronic Structure Theory* Schaefer; H. F., Ed.; Plenum: New York, 1977, p 189.
(20) Pearson, P. K.; Blackman, G. L.; Schaefer, H. F.; Roos, B.; Wahlgren, U. *Astrophys. J. Lett.* **1973**, *184*, L19.
(21) DeFrees, D. J.; McLean, A. D. *Chem. Phys. Lett.* **1986**, *131*, 403.
(22) DeFrees, D. J.; Binkley, J. S.; McLean, A. D. *J. Chem. Phys.* **1984**, *80*, 3720.
(23) Brown, R. D.; Rice, E. H. N. *J. Am. Chem. Soc.* **1984**, *106*, 6475.
(24) DeFrees, D. J.; McLean, A. D. *Chem. Phys. Lett.* **1989**, *158*, 540.
(25) Almlöf, J.; Faegri, K.; Korsell, K. *J. Comput. Chem.* **1982**, *3*, 385. Saebo, S.; Almlöf, J. *Chem. Phys. Lett.* **1987**, *154*, 521.
(26) Meinel, A. B. *J. Astrophys.* **1950**, *111*, 555.
(27) Lambert, D. L.; Brown, J. A.; Hinkle, K. H.; Johnson, H. R. *Astrophys. J.* **1984**, *284*, 223.
(28) Langhoff, S. R.; Jaffe, R. L.; Yee, J. H.; Dalgarno, A. *Geophys. Res. Lett.* **1983**, *10*, 896. Slanger, T. G. *Geophys. Res. Lett.* **1983**, *10*, 130.
(29) Langhoff, S. R.; Bauschlicher, C. W.; Taylor, P. R. *J. Chem. Phys.* **1987**, *86*, 6992.
(30) Bauschlicher, C. W.; Taylor, P. R. *Theor. Chim. Acta* **1988**, *74*, 63.
(31) Langhoff, S. R.; Bauschlicher, C. W.; Taylor, P. R. *J. Chem. Phys.* **1989**, *91*, 5953.
(32) van Duijneveldt, F. B. IBM Research Report No. RJ 945, 1971.
(33) Dunning, T. H. *J. Chem. Phys.* **1989**, *90*, 1007.
(34) Huber, K. P.; Herzberg, G. *Constants of Diatomic Molecules*, Van Nostrand Reinhold: New York, 1979.
(35) Boys, S. F.; Bernardi, F. *Mol. Phys.* **1970**, *19*, 553.
(36) Blomberg, M. R. A.; Siegbahn, P. E. M. *J. Chem. Phys.* **1983**, *78*, 5682. See also Langhoff, S. R.; Davidson, E. R. *Int. J. Quantum Chem.* **1974**, *8*, 61.
(37) Murphy, R. E. *J. Chem. Phys.* **1971**, *54*, 4852.
(38) Turnbull, D. N.; Lowe, R. P. *J. Chem. Phys.* **1988**, *89*, 2763.
(39) Nelson, D. D.; Schiffman, A.; Nesbitt, D. J. *J. Chem. Phys.* **1989**, *90*, 5455.
(40) Werner, H.-J.; Rosmus, P.; Reinsch, E.-A. *J. Chem. Phys.* **1983**, *79*, 905.
(41) Peterson, K. I.; Fraser, G. T.; Klemperer, W. *Can. J. Phys.* **1984**, *62*, 1502.
(42) Hopper, D. G. *J. Chem. Phys.* **1980**, *72*, 3679 and references therein.
(43) Kuo, C.-H.; Beggs, C. G.; Kemper, P. R.; Bowers, M. T.; Leahy, D. J.; Zare, R. N. *Chem. Phys. Lett.* **1989**, *163*, 291.
(44) Heninger, M.; Fenistein, S.; Durup-Ferguson, M.; Ferguson, E. E.; Marx, R.; Mauclaire, G. *Chem. Phys. Lett.* **1986**, *131*, 439.
(45) Werner, H.-J.; Rosmus, P. *J. Mol. Spectrosc.* **1982**, *96*, 362.
(46) Chambaud, G.; Rosmus, P. *Chem. Phys. Lett.* **1990**, *165*, 429.
(47) Partridge, H.; Langhoff, S. R.; Bauschlicher, C. W. *Chem. Phys. Lett.* **1990**, *170*, 13.
(48) Wyttenbach, T.; Beggs, C. G.; Bowers, M. T. *Chem. Phys. Lett.* **1991**, *177*, 239.
(49) Fenistein, S.; Heninger, M.; Marx, R.; Mauclaire, G.; Yang, Y. M. *Chem. Phys. Lett.* **1990**, *172*, 89.
(50) Carter, S.; Handy, N. C. *J. Chem. Phys.* **1987**, *87*, 4294.
(51) Bacic, Z.; Light, J. C. *J. Chem. Phys.* **1987**, *86*, 3065.
(52) Tennyson, J.; Sutcliffe, B. T. *Mol. Phys.* **1986**, *58*, 1067.
(53) (a) Senekowitsch, J.; Carter, S.; Zilch, A.; Werner, H.-J.; Handy, N. C.; Rosmus, P. *J. Chem. Phys.* **1989**, *90*, 783. (b) Comeau, D. C.; Shavitt, I.; Jensen, P.; Bunker, P. R. *J. Chem. Phys.* **1989**, *90*, 6491.
(54) Helgaker, T.; Jørgensen, P. *Adv. Quantum Chem.* **1988**, *19*, 183.
(55) Schaefer, H. F. In *Ion and Cluster Ion Spectroscopy and Structure*; Maier, J. P., Ed.; Elsevier: Amsterdam, 1989; p 109.
(56) Colvin, M. E.; Raine, G. P.; Schaefer, H. F.; Dupuis, M. *J. Chem. Phys.* **1983**, *79*, 1551.
(57) Begemann, M. H.; Gudeman, C. S.; Pfaff, J.; Saykally, R. J. *Phys. Rev. Lett.* **1983**, *51*, 554.
(58) Bauschlicher, C. W.; Taylor, P. R.; Komornicki, A. *J. Chem. Phys.* **1990**, *92*, 3982.
(59) DeVore, T. C.; Gallaher, T. N. *J. Chem. Phys.* **1985**, *82*, 2512.
(60) Beattie, I. R.; Jones, P. J. *J. Chem. Phys.* **1989**, *90*, 5211.
(61) DeVore, T. C. Private communication.
(62) Willetts, A.; Handy, N. C.; Green, W. H.; Jayatilaka, D. *J. Phys. Chem.* **1990**, *94*, 5608. Green, W. H.; Willetts, A.; Jayatilaka, D.; Handy, N. C. *Chem. Phys. Lett.* **1990**, *169*, 127.

(63) Schneider, W.; Thiel, W. *Chem. Phys. Lett.* **1989**, *157*, 367.
(64) Rendell, A. P.; Lee, T. J.; Taylor, P. R. *J. Chem. Phys.* **1990**, *92*, 7050.
(65) Bartlett, R. J.; Cole, S. J.; Purvis, G. D.; Ermler, W. C.; Hsieh, H. C.; Shavitt, I. *J. Chem. Phys.* **1987**, *87*, 6579.
(66) Lee, Y. S.; Bartlett, R. J. *J. Chem. Phys.* **1984**, *80*, 4371.
(67) Ermler, W. C.; Rosenberg, B. J.; Shavitt, I. In *Comparison of Ab Initio Quantum Chemistry with Experiment for Small Molecules*; Bartlett, R. J., Ed.; D. Reidel: Dordrecht, 1985; p 171.
(68) (a) Handy, N. C.; Gaw, J. F.; Simandiras, E. D. *J. Chem. Soc., Faraday Trans.* **1987**, *83*, 1577. (b) Pulay, P.; Lee, J.-G.; Boggs, J. E. *J. Chem. Phys.* **1983**, *79*, 3382.
(69) Lee, T. J.; Bunge, A.; Schaefer, H. F. *J. Am. Chem. Soc.* **1985**, *107*, 137.
(70) Reisenauer, H. P.; Maier, G.; Riemann, A.; Hoffmann, R. W. *Angew. Chem., Int. Ed. Engl.* **1984**, *23*, 641.
(71) Whiting, E. E.; Schadee, A.; Tatum, J. B.; Hougen, J. T.; Nicholls, R. W. *J. Mol. Spectrosc.* **1980**, *80*, 249.
(72) German, K. R.; Bergeman, T. H.; Weinstock, E. M.; Zare, R. N. *J. Chem. Phys.* **1973**, *58*, 4304 and references therein.
(73) Brzozowski, J.; Erman, P.; Lyyra, M. *Phys. Scr.* **1978**, *17*, 507.
(74) Bergeman, T.; Erman, P.; Haratym, Z.; Larsson, M. *Phys. Scr.* **1981**, *23*, 45.
(75) McDermid, I. S.; Laudenslager, J. B. *J. Chem. Phys.* **1982**, *76*, 1824.
(76) Dimpfl, W. L.; Kinsey, J. L. *J. Quant. Spectrosc. Radiat. Transfer* **1979**, *21*, 233.
(77) German, K. R. *J. Chem. Phys.* **1976**, *64*, 4065.
(78) Werner, H.-J.; Rosmus, P.; Schätzl, W.; Meyer, W. *J. Chem. Phys.* **1984**, *80*, 831.
(79) Langhoff, S. R.; van Dishoeck, E. F.; Wetmore, R.; Dalgarno, A. *J. Chem. Phys.* **1982**, *77*, 1379.
(80) Chu, S.-I.; Yoshimine, M.; Liu, B. *J. Chem. Phys.* **1974**, *61*, 5389.
(81) Bauschlicher, C. W.; Langhoff, S. R. *J. Chem. Phys.* **1987**, *87*, 4665.
(82) Coxon, J. A. *J. Mol. Spectrosc.* **1975**, *58*, 1. Coxon, J. A.; Sastry, K. V. L. N.; Austin, J. A.; Levy, D. H. *Can. J. Phys.* **1979**, *57*, 619; Coxon, J. A. *Can. J. Phys.* **1980**, *58*, 933.
(83) Danks, A. C.; Dennefeld, M. *Astronom. J.* **1981**, *86*, 314.
(84) Querci, M.; Querci, F. *Astron. Astrophys.* **1975**, *42*, 329. Gilra, D. P. *Astrophys. J.* **1976**, *203*, 770.
(85) van Dishoeck, E. F.; Black, J. H. *Astrophys. J.* **1982**, *258*, 533.
(86) Bauer, W.; Becker, K. H.; Hubrich, C.; Meuser, R.; Wildt, J. *Astrophys. J.* **1985**, *296*, 758.
(87) Bauer, W.; Becker, K. H.; Bielefeld, M.; Meuser, R. *Chem. Phys. Lett.* **1986**, *123*, 33.
(88) Erman, P.; Lambert, D. L.; Larsson, M.; Mannfors, B. *Astrophys. J.* **1982**, *253*, 983.
(89) McDonald, J. R.; Baronavski, A. P.; Donnelly, V. M. *Chem. Phys.* **1978**, *33*, 161.
(90) van Dishoeck, E. F. *Chem. Phys.* **1983**, *77*, 277.
(91) Chabalowski, C. F.; Peyerimhoff, S. D.; Buenker, R. J. *Chem. Phys.* **1983**, *81*, 57.
(92) ONeil, S. V.; Rosmus, P.; Werner, H.-J. *J. Chem. Phys.* **1987**, *87*, 2847.
(93) Langhoff, S. R.; Bauschlicher, C. W.; Rendell, A. P.; Komornicki, A. *J. Chem. Phys.* **1990**, *92*, 6599.
(94) Bauschlicher, C. W.; Langhoff, S. R. *Theor. Chim. Acta*, in press.
(95) Schiff, B.; Pekeris, C. L. *Phys. Rev. A* **1964**, *3*, 638.
(96) Martin, R. L.; McMurchie, L. E.; Davidson, E. R. *Intern. J. Quantum Chem.* **1978**, *13*, 161.
(97) Hermann, R. *C. R. Acad. Sci. (Paris)* **1951**, *233*, 738.
(98) Carroll, P. K.; Sayers, N. P. *Proc. Phys. Soc. London Sect. A* **1953**, *66*, 1138.
(99) Nadler, I.; Setser, D. W.; Rosenwaks, S. *Chem. Phys. Lett.* **1980**, *72*, 536.
(100) Nadler, I.; Rotem, A.; Rosenwaks, S. *Chem. Phys.* **1982**, *69*, 375.
(101) Nadler, I.; Rosenwaks, S. *J. Chem. Phys.* **1985**, *83*, 3932.
(102) Partridge, H.; Langhoff, S. R.; Bauschlicher, C. W.; Schwenke, D. W. *J. Chem. Phys.* **1988**, *88*, 3174.
(103) Krauss, M.; Neumann, D. B. *Mol. Phys.* **1979**, *37*, 1661.
(104) Huber, K. P.; Vervloet, M. *J. Chem. Phys.* **1988**, *89*, 5957.
(105) Basch, H.; Stevens, W. J.; Krauss, M. *Chem. Phys. Lett.* **1984**, *109*, 212.
(106) Upton, T. H. *J. Phys. Chem.* **1986**, *90*, 754.
(107) Bauschlicher, C. W.; Partridge, H.; Langhoff, S. R.; Taylor, P. R.; Walch, S. P. *J. Chem. Phys.* **1987**, *86*, 7007.
(108) Fu, Z.; Lemire, G. W.; Bishea, G. A.; Morse, M. D. *J. Chem. Phys.* **1990**, *93*, 8420.
(109) Cai, M. F.; Dzugan, T. P.; Bondybey, V. E. *Chem. Phys. Lett.* **1989**, *155*, 430.
(110) Langhoff, S. R.; Bauschlicher, C. W. *J. Chem. Phys.* **1990**, *92*, 1879.
(111) Ginter, D. S.; Ginter, M. L.; Innes, K. K. *Astrophys. J.* **1963**, *139*, 365.
(112) Douglas, M. A.; Hauge, R. H.; Margrave, J. L. *J. Phys. Chem.* **1983**, *87*, 2945.
(113) Abe, H.; Kolb, D. M. *Ber. Bunsenges. Phys. Chem.* **1983**, *87*, 523.
(114) Langhoff, S. R.; Bauschlicher, C. W. *Ann. Rev. Phys. Chem.* **1988**, *39*, 181.
(115) Bauschlicher, C. W.; Langhoff, S. R.; Komornicki, A. *Theor. Chim. Acta.* **1990**, *77*, 263.
(116) Bauschlicher, C. W.; Langhoff, S. R. In *Transition Metal Hydrides*; Dedieu, A., Ed.; VCH Publishers: New York, in press.
(117) Johnson, H. R. *Astrophys. J.* **1982**, *260*, 254.
(118) Littleton, J. E.; Davis, S. P. *Astrophys. J.* **1985**, *296*, 152.
(119) Hammer, P. D.; Davis, S. P. *J. Mol. Spectrosc.* **1979**, *78*, 337.
(120) Simard, B.; Mitchell, S. A.; Humphries, M. R.; Hackett, P. A. *J. Mol. Spectrosc.* **1988**, *129*, 186.
(121) Hammer, P. D.; Davis, S. P. *Astrophys. J.* **1980**, *237*, L51.
(122) Hammer, P. D.; Davis, S. P.; Zook, A. C. *J. Chem. Phys.* **1981**, *74*, 5320.
(123) Phillips, J. G.; Davis, S. P.; Galehouse, D. C. *Astrophys. J.* **1979**, *234*, 401.
(124) Langhoff, S. R.; Bauschlicher, C. W. *Astrophys. J.* **1990**, *349*, 369.
(125) Matos, J. M. O.; Malmqvist, P.-Å.; Roos, B. O. *J. Chem. Phys.* **1987**, *86*, 5032.
(126) Bauschlicher, C. W.; Langhoff, S. R. *J. Chem. Phys.* **1988**, *89*, 2116.
(127) Baltayan, P.; Nedelec, O. *J. Chem. Phys.* **1979**, *70*, 2399.
(128) Fülscher, M. P.; Malmqvist, P.-Å.; Roos, B. O. In *Time-Resolved Laser Spectroscopy in Biochemistry II*; Lakowicz, J. R., Ed.; SPIE Proceeding Series, SPIE: Bellingham, WA, 1990; Vol. 1204,
(129) Malmqvist, P.-Å.; Roos, B. O. *Chem. Phys. Lett.* **1989**, *155*, 189.
(130) Langhoff, S. R.; Bauschlicher, C. W.; Partridge, H. *Intern. J. Quantum Chem. Symp.* **1984**, *18*, 457.
(131) Klotz, R.; Marian, C. M.; Peyerimhoff, S. D.; Hess, B. A.; Buenker, R. J. *Chem. Phys.* **1984**, *89*, 223.
(132) Long, C.; Kearns, D. R. *J. Chem. Phys.* **1973**, *59*, 5729.
(133) Noxon, J. F. *Can. J. Phys.* **1961**, *39*, 1110.
(134) Yarkony, D. R. *J. Chem. Phys.* **1989**, *89*, 7324.
(135) Yarkony, D. R. *J. Chem. Phys.* **1986**, *84*, 2075.
(136) Jensen, J. O.; Yarkony, D. R. *Chem. Phys. Lett.* **1987**, *141*, 391.
(137) Balasubramanian, K.; Pitzer, K. S. *Adv. Chem. Phys.* **1987**, *67*, 287.
(138) Chang, A. H. H.; Pitzer, R. M. *J. Am. Chem. Soc.* **1989**, *111*, 2500.
(139) Morokuma, K. Private communication.